91602
new 82-10

LEGAL NOTICE

This report was prepared by Ontario Hydro and, while effort has been made to assure the accuracy and applicability of the material contained herein, neither Ontario Hydro nor any person acting on its behalf:

(a) makes any warranty, express or implied with respect to the use of any information, apparatus, method or process disclosed in this report or that such use may not infringe privately owned rights, or

(b) assumes any liabilities with respect to the use of, or for damages resulting from the use of, any information, apparatus, method or process disclosed in this report.

ontario hydro
research division

COMPLIMENTARY COPY
Please Credit Ontario Hydro Research if Reproduced in Whole or in Part

EVALUATION OF CRACKS IN THE LAMBTON TGS UNIT 3 BOILER CIRCULATION PUMP CASINGS AND DISCHARGE VALVE BODIES

Report No. 88-282-K

D.A. Scarth
Nondestructive and Fracture Evaluation Section
Metallurgical Research Department

ABSTRACT

Cracks have been found in the boiler circulation pump casings and discharge valve bodies in Lambton TGS Unit 3. The deepest cracks not repaired in the pump casing are 3 mm deep, and the deepest cracks not repaired in the discharge valve bodies are 10 mm deep. An evaluation of the structural integrity of both components with cracks of various depths has been completed. The safety margins against fracture initiation and against plastic collapse for the existing cracks are all above 4.0. The existing detected cracks are acceptable for continued service. The deepest crack detected in the pump casings, and subsequently repaired, was 77% through the wall thickness. The safety margins for this crack under normal operating pressure was 1.82 for fracture initiation, and 1.68 for plastic collapse. The deepest crack detected in the discharge valve bodies, and subsequently repaired, was 55% through the wall thickness. The safety margins for this crack under normal operating pressure was 2.89 for fracture initiation, and 3.48 for plastic collapse. It was recommended that all of the boiler circulation pumps and discharge valves be subjected to periodic hydrostatic tests, and be monitored by means of a periodic inspection program.

job	file	date	report no.
83-299-872	826.242	November 14, 1988	88-282-K

91602
new 82-10

ontario hydro
research division

EXECUTIVE SUMMARY

EVALUATION OF CRACKS IN THE LAMBTON TGS UNIT 3 BOILER CIRCULATION PUMP CASINGS AND DISCHARGE VALVE BODIES

Report No. 88-282-K

D.A. Scarth
Nondestructive and Fracture Evaluation Section
Metallurgical Research Department

Cracks have been found in the boiler circulation pump casings and discharge valve bodies in Lambton TGS Unit 3. Any cracks in a pump casing deeper than 3 mm were repaired, and any cracks in a discharge valve body deeper than 10 mm were repaired. An evaluation of the structural integrity of the pump casings and discharge valve bodies containing cracks of various depths was performed. The purpose of the evaluation was to determine the acceptability of the remaining detected cracks for continued service, as well as to estimate the safety margins which existed for the deeper cracks which were detected and repaired. Safety margins have been calculated for a range of crack depths to enable the assessment of any cracks which may be detected in pump casings and discharge valve bodies in the future.

Safety margins against fracture initiation, and against plastic collapse were calculated for various crack depths. The safety margins for the 3 mm deep cracks in the pump casings and the 10 mm deep cracks in the discharge valve bodies are all above 4.0. The detected cracks which remain in the circulation pump casings and discharge valve bodies of Lambton TGS Unit 3 are acceptable for continued service. The deepest crack detected in the pump casings, and subsequently repaired, was 77% through the wall thickness. The safety margins for this crack under normal operating pressure was 1.82 for fracture initiation, and 1.68 for plastic collapse. The deepest crack detected in the discharge valve bodies, and subsequently repaired, was 55% through the wall thickness. The safety margins for this crack under normal operating pressure was 2.89 for fracture initiation, and 3.48 for plastic collapse.

job	file	date	report no.
83-299-872	826.242	November 14, 1988	88-282-K

It was recommended that the circulation pumps and discharge valves in all the units in the Lambton TGS should be periodically subjected to a hydrostatic test. As well, the circulation pumps and discharge valves in all the Lambton units should be monitored in the future by means of a periodic inspection program.

The mechanism of crack growth has not been identified. Mechanical fatigue crack growth due to startup/shutdown cycles was found to be insignificant. The cause of the extent of the subcritical crack growth should be identified.

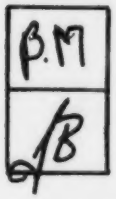

TABLE OF CONTENTS

		Page
1.0	INTRODUCTION	1
2.0	CONCLUSIONS	7
3.0	RECOMMENDATIONS	7
4.0	MATERIAL PROPERTIES	7
4.1	Tensile Properties	8
4.2	Fracture Toughness K_{Ic}	8
4.3	Thermal Properties	9
5.0	STRESSES	11
5.1	Mechanical Stresses in the Pump Casing	11
5.2	Primary Stress in the Pump Casing	12
5.3	Mechanical Stresses in the Discharge Valve Body	13
5.4	Thermal Stresses	13
5.4.1	Steady-State Thermal Stresses	13
5.4.2	Transient Thermal Stresses	14
6.0	CRACK-TIP STRESS INTENSITY FACTORS	23
7.0	LIMIT LOAD ANALYSIS	25
7.1	Limit Load Analysis for the Pump Casing	25
7.2	Limit Load Analysis for the Discharge Valve Body	25
8.0	FATIGUE CRACK GROWTH	26
9.0	EVALUATION OF SAFETY MARGINS	29
9.1	Safety Margins on the Crack-Tip Stress Intensity Factor	29
9.1.1	Safety Margins for the Pump Casing	30
9.1.2	Safety Margins for the Discharge Valve Body	30
9.2	Safety Margins Against Plastic Collapse	31
9.2.1	Safety Margins for the Pump Casing	31
9.2.2	Safety Margins for the Discharge Valve Body	31
9.3	Recommendations	31
10.0	ACKNOWLEDGEMENTS	32
REFERENCES		33

		Page
APPENDIX A	Details of the Calculation of Mechanical Stresses in the Pump Casing	49
APPENDIX B	Formulae for the Crack-Tip Stress Intensity Factor	61
APPENDIX C	Crack Growth Due to Mechanical Fatigue	66
DISTRIBUTION		last page

LIST OF TABLES

TABLE 4–1 Material Properties

TABLE 4–2 Weight Percent Chemical Compositions of Cast Steels

TABLE 4–3 Fracture Toughness of Lakeview TGS A216 WCB Cast Steel Valve Flange

TABLE 5–1 Mechanical Stress Coefficients for the Pump Casing for an Internal Pressure of 17.0 MPa

TABLE 5–2 Coefficients for Transient Thermal Stresses

TABLE 9–1 Minimum Safety Margins for the Boiler Circulation Pump Casing, Based on the Hydrostatic Test Pressure of 22.0 MPa

TABLE 9–2 Minimum Safety Margins for the Boiler Circulation Pump Discharge Valve Body, Based on the Hydrostatic Test Pressure of 22.0 MPa

TABLE A–1 Normalized Normal Stress Coefficients for the Cubic Stress Distribution for the Pump Casing

TABLE B–1 Geometry Influence Coefficients for an Axial Crack With an Infinite Aspect Ratio Subject to a Cubic Hoop Stress Distribution (From Reference /12/)

TABLE B–2 Geometry Influence Coefficients for an Axial Crack With an Aspect Ratio of 10 Subject to a Cubic Hoop Stress Distribution (From Reference /13/)

LIST OF FIGURES

FIGURE 1–1	Schematic of boiler circulation pump and suction manifold.
FIGURE 1–2	Boiler circulation pump.
FIGURE 1–3	Pump casing containing cracks.
FIGURE 1–4	Pump discharge valve body.
FIGURE 5–1	Major dimensions of pump casing profiles.
FIGURE 5–2	Distribution of normal stress in the pump casing at Profile 1 in the upper corner region for steady state and cooldown conditions.
FIGURE 5–3	Distribution of normal stress in the pump casing at Profile 2 in the midsection region for steady state and cooldown conditions.
FIGURE 5–4	Distribution of hoop stress in the discharge valve body with a wall thickness of 47 mm for steady state and cooldown conditions.
FIGURE 5–5	Distribution of hoop stress in the discharge valve body with a wall thickness of 64 mm for steady state and cooldown conditions.
FIGURE 5–6	Cold start, load changes and shutdown histories for Lambton TGS Unit 2.
FIGURE 5–7	Illustration of idealized temperature distribution.
FIGURE 6–1	Shapes of axial cracks in a cylinder modelled in the evaluation.
FIGURE 8–1	Reference fatigue crack growth curves for carbon and low alloy ferritic steels (from Reference /17/).
FIGURE 9–1	Variation of the margin on the crack–tip stress intensity factor with crack depth for a crack with an infinite crack aspect ratio at Profile 1 in the pump casing.
FIGURE 9–2	Variation of the margin on the crack–tip stress intensity factor with crack depth for a crack with a crack aspect ratio of 10 to 1 at Profile 1 in the pump casing.
FIGURE 9–3	Variation of the margin on the crack–tip stress intensity factor with crack depth for a crack with an infinite crack aspect ratio at Profile 2 in the pump casing.
FIGURE 9–4	Variation of the margin on the crack–tip stress intensity factor with crack depth for a crack with a crack aspect ratio of 10 to 1 at Profile 2 in the pump casing.

FIGURE 9–5 Variation of the margin on the crack–tip stress intensity factor with crack depth for a crack with an infinite crack aspect ratio in a discharge valve body with a wall thickness of 47 mm.

FIGURE 9–6 Variation of the margin on the crack–tip stress intensity factor with crack depth for a crack with a crack aspect ratio of 10 to 1 in a discharge valve body with a wall thickness of 47 mm.

FIGURE 9–7 Variation of the margin on the crack–tip stress intensity factor with crack depth for a crack with an infinite crack aspect ratio in a discharge valve body with a wall thickness of 64 mm.

FIGURE 9–8 Variation of the margin on the crack–tip stress intensity factor with crack depth for a crack with a crack aspect ratio of 10 to 1 in a discharge valve body with a wall thickness of 64 mm.

FIGURE 9–9 Variation of the margin against plastic collapse with crack depth for a crack with an infinite aspect ratio at Profile 2 in the pump casing.

FIGURE 9–10 Variation of the margin against plastic collapse with crack depth for a crack with an aspect ratio of 10 to 1 at Profile 2 in the pump casing.

FIGURE 9–11 Variation of the margin against plastic collapse with crack depth for a crack with an infinite aspect ratio in a discharge valve body with a wall thickness of 47 mm.

FIGURE 9–12 Variation of the margin against plastic collapse with crack depth for a crack with an infinite aspect ratio in a discharge valve body with a wall thickness of 64 mm.

FIGURE A–1 Illustration of superposition of stresses.

FIGURE A–2 Axisymmetric finite element model of Profile 1 of the pump casing.

FIGURE A–3 Axisymmetric finite element model of Profile 2 of the pump casing.

FIGURE A–4 Normalized normal stress distribution in the pump casing at Profile 1 – upper corner for internal pressure on the inside wall.

FIGURE A–5 Normalized normal stress distribution in the pump casing at Profile 1 – upper corner for tension on the suction end.

FIGURE A–6 Normalized normal stress distribution in the pump casing at Profile 2 – midsection for internal pressure on the inside wall.

FIGURE A–7 Normalized normal stress distribution in the pump casing at Profile 2 – midsection for tension on the suction end.

FIGURE C-1 Integrated fatigue crack growth for Profile 1 in the pump casing.

FIGURE C-2 Integrated fatigue crack growth for Profile 2 in the pump casing.

FIGURE C-3 Integrated fatigue crack growth for a discharge valve body with a wall thickness of 47 mm.

FIGURE C-4 Integrated fatigue crack growth for a discharge valve body with a wall thickness of 64 mm.

FIGURE C-5 Illustration of estimation of fatigue crack growth.

ontario hydro
research division

To

Mr. R.W. Patterson
Manager
Chemistry and Metallurgy
Central Thermal Services
Technical and Training Services

EVALUATION OF CRACKS IN THE LAMBTON TGS UNIT 3 BOILER CIRCULATION PUMP CASINGS AND DISCHARGE VALVE BODIES

1.0 INTRODUCTION

Water in the Lambton TGS boilers is circulated to the bottom of the boiler by means of eight downcomer pipes. A suction manifold is suspended from these downcomers as shown in Figure 1-1. Four single suction/double discharge centrifugal circulation pumps, with attached pump motors and eight discharge lines (two for each pump) are suspended from the suction manifold. The circulation pump is illustrated in Figure 1-2. Cracks have been detected on the inside wall of some of the pump casings and discharge valve bodies in Unit 3.

The locations of the major cracks in the cast steel pump casings are shown in Figure 1-3. The major cracks were characterized as intermittent surface cracks and followed a circumferential path in the horizontal plane around the volute of the pump casings. The deepest crack was in the upper corner region of the volute and was sized by grinding to be about 75 mm deep (77% through the 97 mm wall thickness) and 430 mm long. All cracks deeper than 3 mm were ground out, and weld repaired where the wall thickness dropped below a minimum wall thickness.

A schematic illustration of the cross-section of the cast steel discharge valve body is shown in Figure 1-4. The major cracks were characterized as intermittent surface cracks orientated axially in the valve bodies. The deepest crack was 55% through the 64 mm wall thickness. All cracks deeper than 10 mm were ground out, and weld repaired where the wall thickness dropped below a minimum wall thickness.

It is believed that these cracks initiated as casting defects. A structural integrity "leak-before-break" evaluation of postulated through-wall cracks in the discharge valve bodies was previously performed by the Chemistry and Metallurgy Department of Central Thermal Services/1/. A structural integrity evaluation of the pump casings and discharge valve bodies containing cracks of various depths has been performed by the Fracture Mechanics Unit at the request of the Chemistry and Metallurgy Department of Central Thermal Services. This report contains a summary of the evaluation.

The purpose of this evaluation was to determine the acceptability of the remaining detected cracks for continued service, as well as to estimate the safety margins which existed for the deeper cracks which were detected and repaired. Safety margins have been calculated for a range of crack depths to enable the assessment of any cracks which may be detected in pump casings and discharge valve bodies in the future.

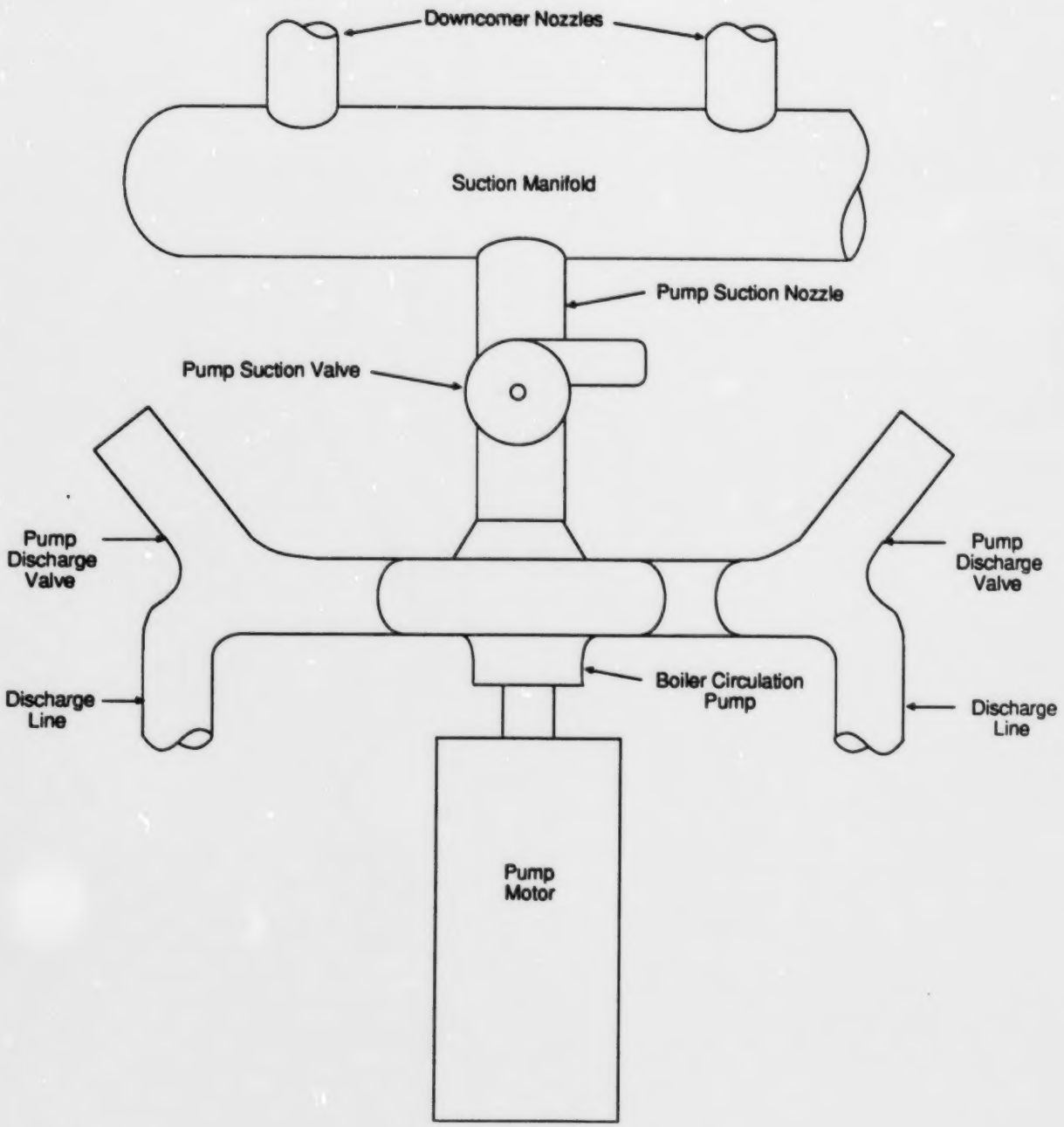

FIGURE 1-1 **Schematic of Boiler Circulation Pump and Suction Manifold**

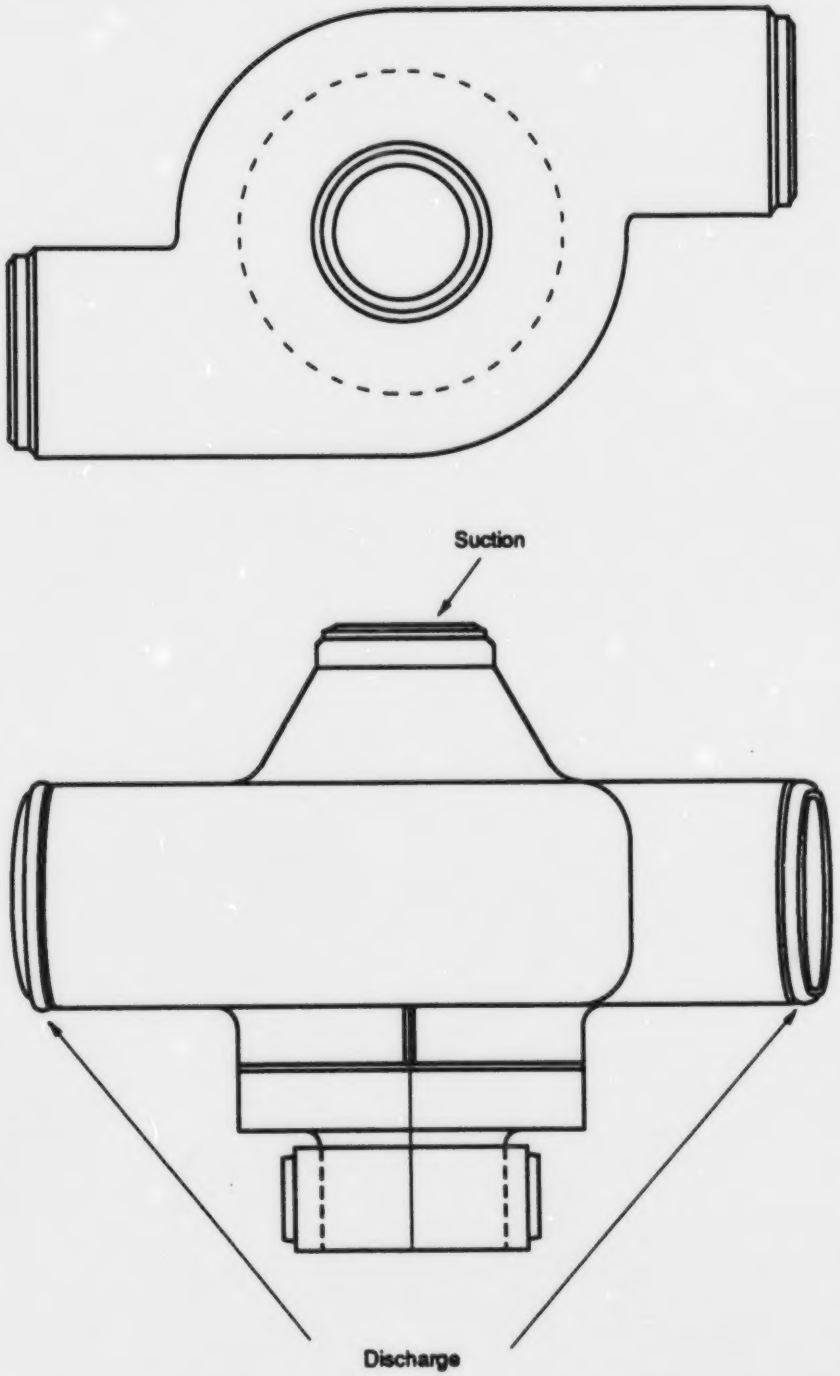

FIGURE 1-2 **Boiler circulation pump.**

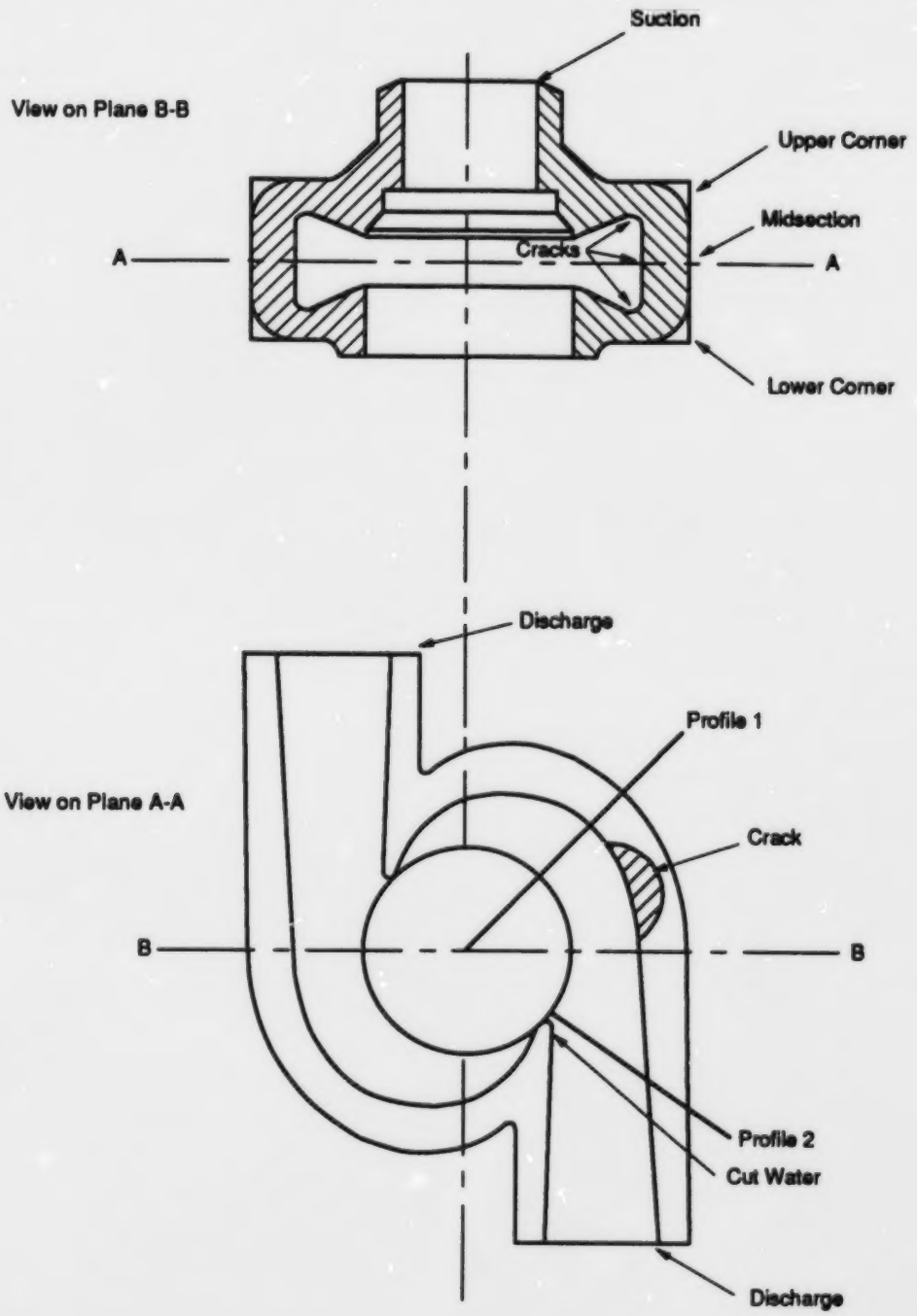

FIGURE 1-3 Pump casing containing cracks.

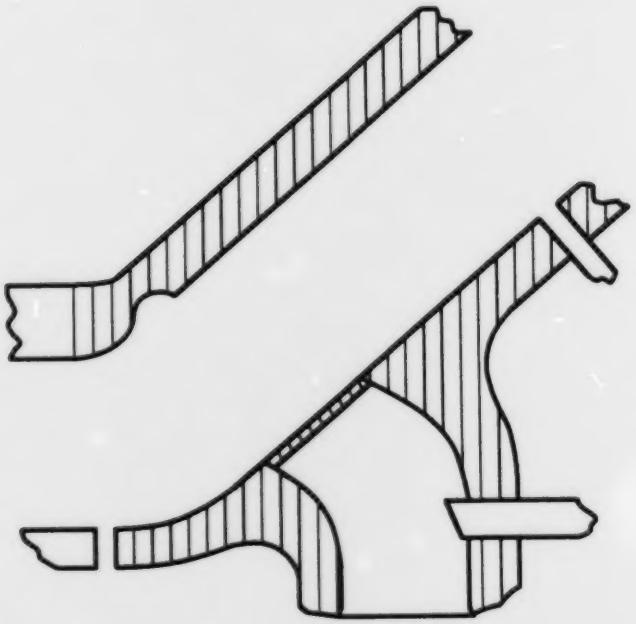

FIGURE 1-4 **Pump discharge valve body.**

2.0 CONCLUSIONS

(a) An evaluation of the structural integrity of the boiler circulation pump casings and discharge valve bodies with cracks of various depths in Lambton TGS Unit 3 has been completed.

(b) The deepest cracks remaining in the circulation pump casings are 3 mm deep. The safety margins against fracture initiation and against plastic collapse are greater than 4.0 for pressures up to the hydrostatic test pressure. The deepest crack detected in a pump casing, and subsequently repaired, was 77% through the wall thickness. The safety margin for this crack against fracture initiation was predicted to be 1.82 for the normal operating pressure, and 1.42 for the hydrostatic test pressure. The safety margin against plastic collapse was predicted to be 1.68 for the normal operating pressure, and 1.43 for the hydrostatic test pressure.

(c) The deepest cracks remaining in the discharge valve bodies are 10 mm deep. The safety margins against fracture initiation and against plastic collapse are greater than 4.0 for pressures up to the hydrostatic test pressure. The deepest crack detected in a discharge valve body, and subsequently repaired, was 55% through the wall thickness. The safety margin for this crack against fracture initiation was predicted to be 2.89 for the normal operating pressure, and 2.26 for the hydrostatic test pressure. The safety margin against plastic collapse was predicted to be 3.48 for the normal operating pressure, and 2.97 for the hydrostatic test pressure.

(d) The mechanism of crack growth has not been identified. Mechanical fatigue crack growth due to startup/shutdown cycles was found to be insignificant.

(e) The inspected boiler circulation pump casings and discharge valve bodies in Lambton TGS Unit 3 are acceptable for continued service. Recommendations are given below.

3.0 RECOMMENDATIONS

(a) The detected cracks which remain in the boiler circulation pump casings and discharge valve bodies of Lambton TGS Unit 3 are acceptable for continued service.

(b) The circulation pumps and discharge valves in all the units in the Lambton TGS should be periodically subjected to a hydrostatic test at a pressure of 22.0 MPa.

(c) The circulation pumps and discharge valves in all the units in the Lambton TGS should be subjected to a periodic inspection.

(d) The cause of the extent of the subcritical crack growth should be identified.

4.0 MATERIAL PROPERTIES

The pump casings and discharge valves are composed of A216 WCB cast and normalized steel. The castings were normalized at 900°C and air cooled.

4.1 Tensile Properties

Young's modulus, the yield stress, ultimate stress and flow stress are given in Table 4-1 for the hydrostatic test temperature of 25°C and the design operating temperature of 366°C. Young's modulus, the yield stress and ultimate stress were taken to be the minimum requirements given in ASME Section III, Division 1, Appendix 1/2/. The room temperature yield and ultimate stresses are the same as given in ASME Section II, Part A/3/. The flow stress was taken to be the average of the yield and ultimate stresses.

4.2 Fracture Toughness K_{Ic}

Material from an A216 WCB pump casing was not available for fracture toughness testing. Material taken from an A216 WCB cast and normalized valve flange from the Lakeview TGS was used to obtain fracture toughness values. The chemical composition of samples taken from a Lambton pump casing and the Lakeview valve flange were determined/4,5/ and are compared in Table 4-2. The carbon and sulphur content of the pump casing material is higher than that of the valve flange, which generally indicates that the pump casing would have a lower fracture toughness at room temperature than the valve flange. The pump casing has a design minimum wall thickness at manufacture of 91 mm, while the valve flange had a thickness of 43 mm. The thicker walled pump casing would be expected to have a coarser grain structure at mid-thickness than in the valve flange, which is also generally associated with a lower fracture toughness.

Fracture toughness tests were performed on the A216 WCB valve flange material at 25°C, 340°C and 364°C/6/ by following the 1987 ASTM E813 standard/7/. The tests were carried out on 25 mm thick three-point bend specimens. The resulting values of the J-integral at initiation, J_{Ic}, were given in /6/, and were converted to K_{Ic} by using

$$K_{Ic} = (J_{Ic}\, E/(1-\nu^2))^{0.5} \qquad (4-1)$$

where E is Young's modulus and ν is Poisson's ratio, = 0.3. The resultant values of K_{Ic} are given in Table 4-3. The lowest value for K_{Ic} at room temperature is 161 MPa $\sqrt{m}$, and the lowest value at operating temperature is 133 MPa $\sqrt{m}$. The room temperature tests exhibited ductile tearing with intermittent cleavage/6/, indicating that room temperature is in the middle of the ductile-to-brittle transition temperature range. Typically, values of fracture toughness in this temperature range measured from thicker specimens (eg. 100 mm thick) will be lower than fracture toughness values measured from 25 mm thick specimens/6/.

Room temperature fracture toughness values for cast steels following British standards are given in /8/. The steel whose chemical composition most closely matches the composition of A216 WCB is denoted as steel A in /8/. The composition of steel A is given in Table 4-2. The room temperature fracture toughness of steel A is given in /8/ as 140 MPa $\sqrt{m}$. The fracture tests were performed on three-point bend specimens with thicknesses of 25 and 30 mm.

From the above results, a value for the fracture toughness of the pump casing and discharge valve body for the range in temperature of 25°C to 366°C was estimated to be 120 MPa $\sqrt{m}$. At 25°C this value is considered to be a "best estimate", and not a known lower bound. This value is considered to be a lower-bound measure of fracture toughness at the upper shelf temperature of 366°C, due to the blunting of the crack tip.

4.3 Thermal Properties

The coefficient of thermal expansion, α, was taken from ASME Section III, Appendix I/2/.

TABLE 4-1

Material Properties

Property	Temperature	
	25°C	366°C
Young's Modulus, E (MPa)	206×10^3	175×10^3
Poisson's Ratio, ν	0.3	0.3
Yield Stress, σ_{ys} (MPa)	248	179
Flow Stress, σ_f (MPa)	366	331
Ultimate Stress, σ_u (MPa)	483	483
Fracture Toughness, K_{Ic} (MPa $\sqrt{m}$)	120	120
Coefficient of Thermal Expansion, α ($1/°C$)	11.54×10^{-6}	15.03×10^{-6}

TABLE 4-2

Weight Percent Chemical Compositions of Cast Steels

Sample	C	P	S	Mn	Si	Ni	Mo	V	Cu	Al	Cr
A216 WCB from pump casing	0.24	0.05	0.037	0.57	-	0.18	0.065	0.1	0.14	0.06	0.22
A216 WCB from valve flange	0.19	0.003	0.018	0.56	0.22	0.081	0.021	0.002	-	-	0.12
Steel A in ref. /8/	0.24	0.022	0.008	1.26	0.40	-	-	-	-	-	-

TABLE 4-3

Fracture Toughness of Lakeview TGS
A216 WCB Cast Steel Valve Flange

Test Temperature (°C)	K_{Ic} from Following ASTM E813-87 (MPa $\sqrt{m}$)	K_{Ic} from Stretch Zone Width Measurements[+] (MPa $\sqrt{m}$)	
		Minimum	Average
24	–	161	195
24	181	–	–
340	147	–	–
364	158	133	175

[+]See reference /6/.

5.0 STRESSES

The stresses used in the evaluation were the stresses acting normal to the surface of the crack in the uncracked component. Both mechanical stresses and thermal stresses were considered. The mechanical stresses due to internal pressure and the weight of the motor suspended from the pump casing were calculated. Stresses due to loads applied to the discharge valve ends were not addressed. The mechanical loads are summarized as follows:

i) Internal pressure
- 8.5 MPa, cooldown
- 17.0 MPa, normal operating pressure
- 18.0 MPa, operating overpressure for maximum power output
- 19.7 MPa, minimum safety valve setting pressure
- 22.0 MPa, hydrostatic test pressure
- 23.8 MPa, 1.4 x normal operating pressure

ii) Deadweight load due to pump motor of 100,000 N. This load is applied to the pump casing only.

5.1 Mechanical Stresses in the Pump Casing

The pump casing was idealized as being axisymmetric. The radius of the casing profile in the radial-vertical plane was varied, with the angular position about the major axis of the casing, of the particular radial-vertical slice through the cross-section. Stresses were calculated by two-dimensional linear elastic finite element

analysis by using the commercial computer code ABAQUS/9/. The stresses were calculated for two profiles (slices) as illustrated in Figure 1-3. Profile 1 is representative of the region at approximately 45° from the cutwater, while Profile 2 is at the cutwater. Major dimensions for each profile are given in Figure 5-1. The wall thickness of the pump casings varied. The wall thickness of the volute at Profile 1 was taken to be the design minimum wall thickness of 91 mm. The wall thickness for Profile 2 was taken to be 88 mm for the stress analysis. For the calculation of the crack-tip stress intensity factor, the wall thickness of Profile 2 was assumed to be 91 mm, to be consistent with Profile 1. Referring to Figure 1-3, the maximum normal stress distribution in each of the three regions denoted as "upper corner", "midsection" and "lower corner" were determined for both profiles. Details of the stress analysis are given in Appendix A of this report.

The location of the maximum normal stress distribution at Profile 1 was in the upper corner region, and is plotted in Figure 5-2 for the normal operating pressure of 17.0 MPa. The location of the maximum stress distribution at Profile 2 was in the midsection region, and is plotted in Figure 5-3 for 17.0 MPa. The weight of the pump motor accounted for about 1% of the stress, and the mechanical stress values can therefore be scaled with respect to internal pressure. The nonlinear stress distributions were fit by using least-squares to the cubic equation

$$\sigma_p = A_0 + A_1 x + A_2 x^2 + A_3 x^3 \qquad (5\text{-}1)$$

where σ_p - the stress acting normal to the crack surfaces,

x - the distance from the inside wall in metres,

A_i - stress coefficients which are a function of internal pressure.

The coefficients A_i for the normal operating pressure of 17.0 MPa are given in Table 5-1. The coefficients for other pressures were scaled with respect to pressure.

5.2 Primary Stress in the Pump Casing

The primary stresses are used as input to the limit load (net-section plastic collapse) analysis. The primary stresses oppose the external forces on the pump casing, which in this case are the internal pressure and deadweight. The membrane stress due to internal pressure and deadweight were included, but the through-wall bending stress was not included. This is due to the bending stress being induced by the gross structural discontinuity of the pump casing and is self-limiting; the bending stress is not required to maintain equilibrium with the external forces in the casing.

The pump casing was again idealized as being axisymmetric with the radius depending on the angular location of the profile in the horizontal plane. The average membrane stress is then given by treating the pump casing as a thin-walled cylinder with closed ends under internal pressure.

$$\sigma_{prim} = p\, R_{imax}/(2t_{min}) \qquad (5\text{-}2)$$

where p - internal pressure,

R_{imax} = maximum bowl radius for the profile,

t_{min} = minimum bowl wall thickness for the profile.

5.3 Mechanical Stresses in the Discharge Valve Body

The valve body was idealized as a circular cylinder under internal pressure. This excludes the applicability of this evaluation to cracks located where the stresses on the crack are dominated by any three-dimensional stress raisers in the valve body. External loads from the discharge lines were not addressed. The stress acting normal to the crack surface is the hoop stress. The hoop stress distribution was calculated by using Lame's solution/10/.

$$\sigma_p = \frac{p \; R_i^2}{(R_o^2 - R_i^2)} (1 + (R_o/r)^2) \qquad (5\text{-}3)$$

where R_i = the inner wall radius,

R_o = the outer wall radius,

r = the radial coordinate.

Calculations were performed for the following dimensions:

Inner Radius	Wall Thickness
152 mm	47 mm
152 mm	64 mm

The wall thickness of 47 mm is the design minimum wall thickness, while 64 mm is the minimum wall thickness measured/1/. The hoop stress distribution for the normal operating pressure of 17.0 MPa for a wall thickness of 47 mm is plotted in Figure 5-4, and for a wall thickness of 64 mm in Figure 5-5.

5.4 Thermal Stresses

5.4.1 Steady-State Thermal Stresses

The outside walls of the pump casings and discharge valves are covered by about 50 mm of insulation. A simple steady-state one-dimensional thermal analysis based on concentric cylinders yielded a temperature difference across the pump casing wall of only 1.8°C. The heat transfer calculations are not given in this report.

Temperature differences across the wall of the discharge valve body have been measured for Unit 2, and are given in Figure 5-6. The negligible temperature difference across the wall thickness during steady state is confirmed in the figure. Therefore, steady-state thermal stresses are insignificant.

5.4.2 Transient Thermal Stresses

The plot of the inner and outer wall surface temperatures of the discharge valve body in Figure 5-6 show a maximum temperature difference across the wall during the cooldown transient of about 20°C. The inside wall surface is cooler than the outside wall surface during cooldown, and the thermal stress due to the through-wall temperature gradient would be tension on the inside surface. Since the temperature distribution through the wall is not known, it is assumed that the temperature distribution is linear. Based on the ratio of the wall thickness of the pump casing to the wall thickness of the valve body, = 91/64, it was also assumed that the maximum temperature difference across the wall thickness of the pump casing during cooldown was 30°C. The pressure at this point in the transient is 8.5 MPa.

The distribution of thermal stress through the wall thickness was taken to be that given for a flat plate under full transverse constraint with a linear through-thickness temperature profile. For the temperature distribution given in Figure 5-7 this is given by /10/

$$\sigma_{th} = \alpha E(\Delta T_1/2)(1 - 2x/t)/(1-\nu) \qquad (5\text{-}4)$$

where α = coefficient of thermal expansion,

ΔT_1 = temperature difference across the wall thickness,

x = distance from the inside wall,

t = wall thickness.

The thermal stress was written in the form

$$\sigma_{th} = A_{th0} + A_{th1}\, x \qquad (5\text{-}5)$$

where

$$A_{th0} = \alpha E(\Delta T_1/2)/(1-\nu) \qquad (5\text{-}6)$$

$$A_{th1} = -2\alpha E(\Delta T_1/2)/(t(1-\nu)) \qquad (5\text{-}7)$$

The coefficients A_{thi} for the pump casing and valve body are given in Table 5-2.

The distribution of the combined thermal and mechanical normal stress in the pump casing during cooldown at a pressure of 8.5 MPa is given in Figure 5-2 for Profile 1 in the upper corner region, and Figure 5-3 for Profile 2 in the midsection region. The normal stresses during steady state normal operating (pressure = 17.0 MPa) are still higher than the stresses during cooldown, and thermal stresses in the pump casing will not be considered any further in this evaluation. The combined thermal and mechanical hoop stress distribution in the discharge valve body during cooldown is given in Figure 5-4 for a wall thickness of 47 mm and Figure 5-5 for a wall thickness of 64 mm. The stresses during cooldown are greater than the steady-state normal operating stresses near the inside wall. Therefore, thermal stresses during cooldown will be included in the flaw evaluation of the discharge valve bodies.

TABLE 5-1

Mechanical Stress Coefficients for the Pump Casing
for an Internal Pressure of 17.0 MPa

Location	Stress Coefficients			
	A_0 (MPa)	A_1 (MPa/m)	A_2 (MPa/m^2)	A_3 (MPa/m^3)
Profile 1 – Upper Corner	161.8	-6314	9.433×10^4	-5.013×10^5
Profile 2 – Midsection	155.5	-3495	2.377×10^4	-9.320×10^4

TABLE 5-2

Coefficients for Transient Thermal Stresses

Component	Wall Thickness (mm)	A_{th0} (MPa)	A_{th1} (MPa/m)
Pump Casing	91	57.01	-1247
Valve Body	47	38.00	-1628
Valve Body	64	38.00	-1188

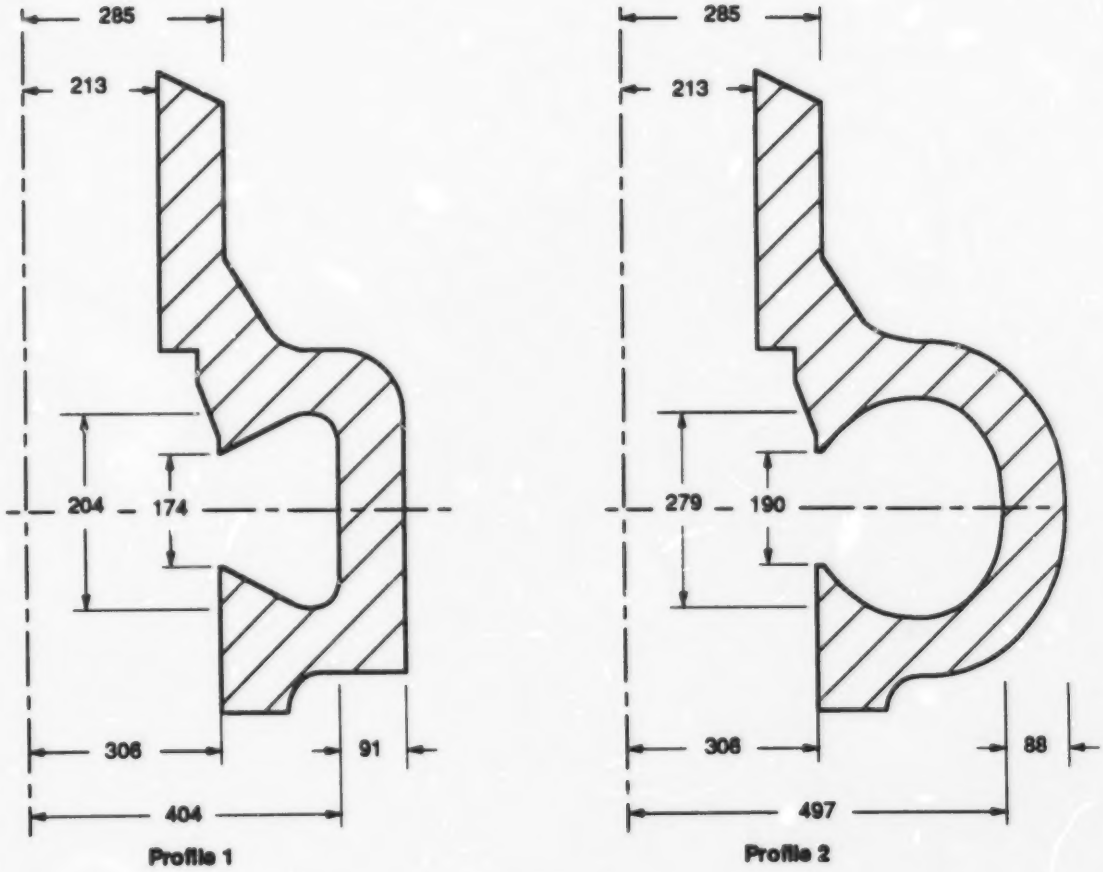

FIGURE 5-1 Major dimensions of pump casing profiles.

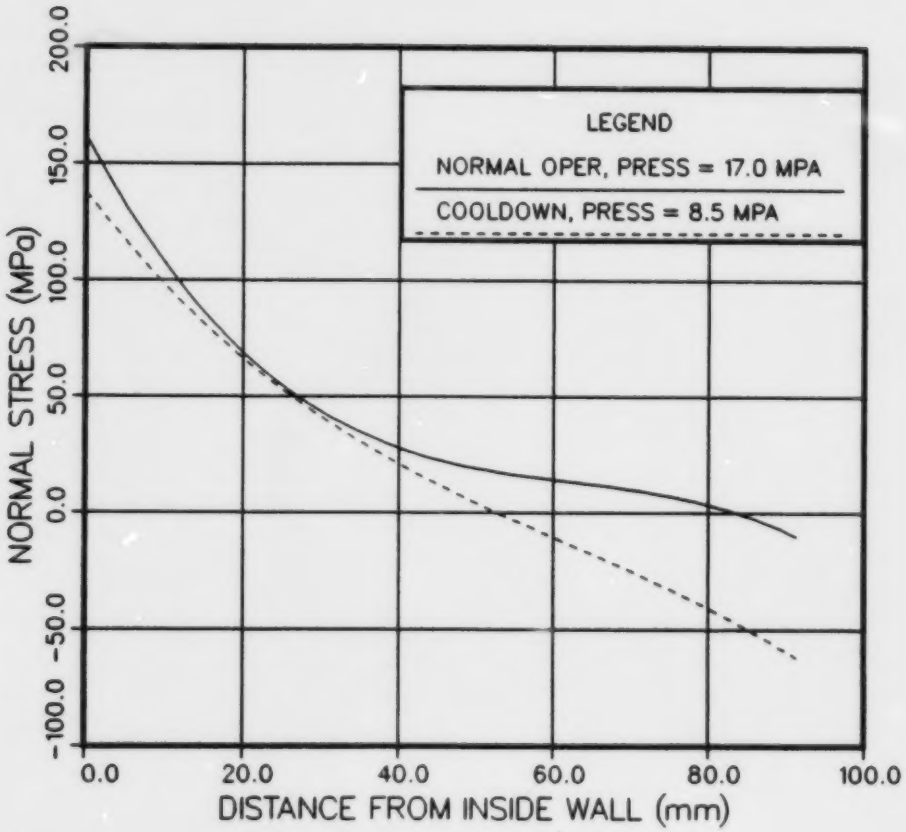

FIGURE 5-2 **Distribution of normal stress in the pump casing at Profile 1 in the upper corner region for steady state and cooldown conditions.**

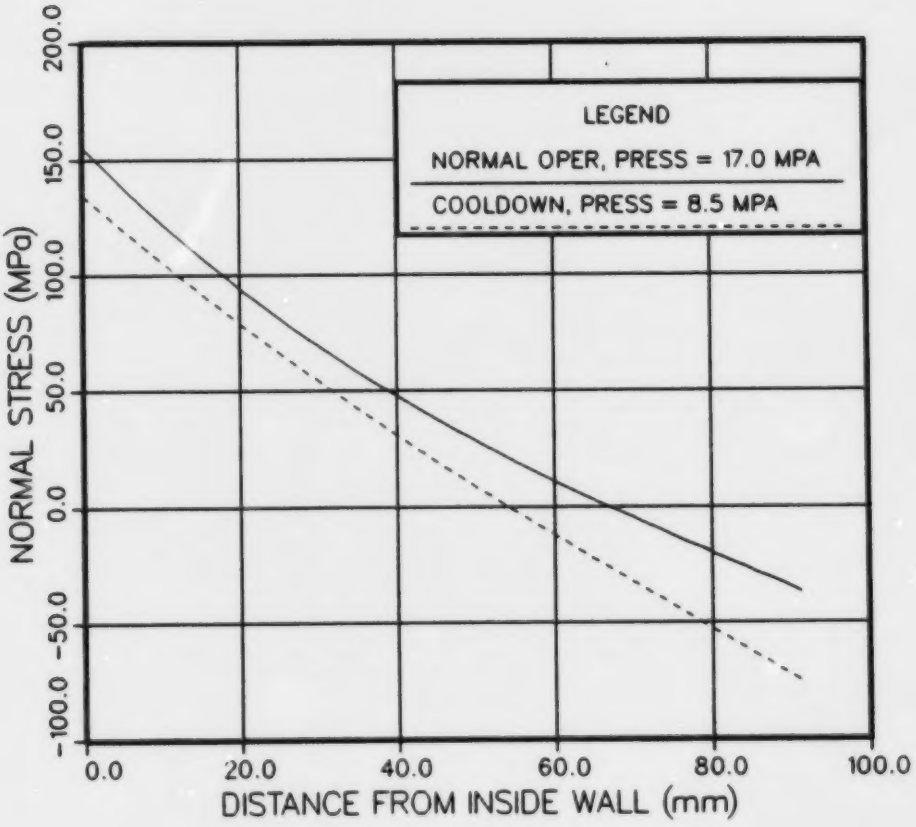

FIGURE 5-3 **Distribution of normal stress in the pump casing at Profile 2 in the midsection region for steady state and cooldown conditions.**

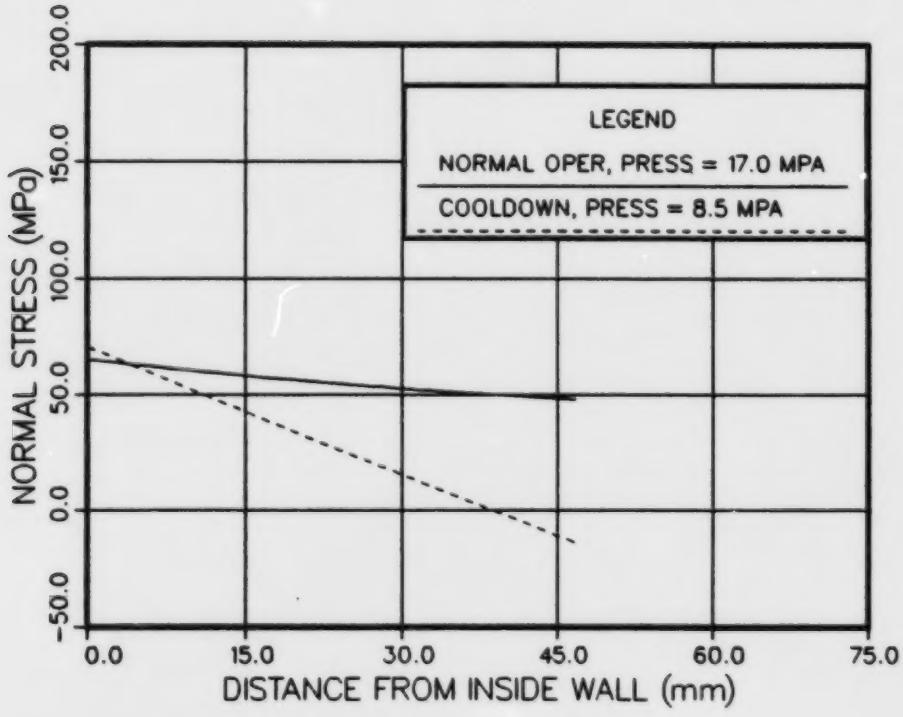

FIGURE 5-4 **Distribution of hoop stress in the discharge valve body with a wall thickness of 47 mm for steady state and cooldown conditions.**

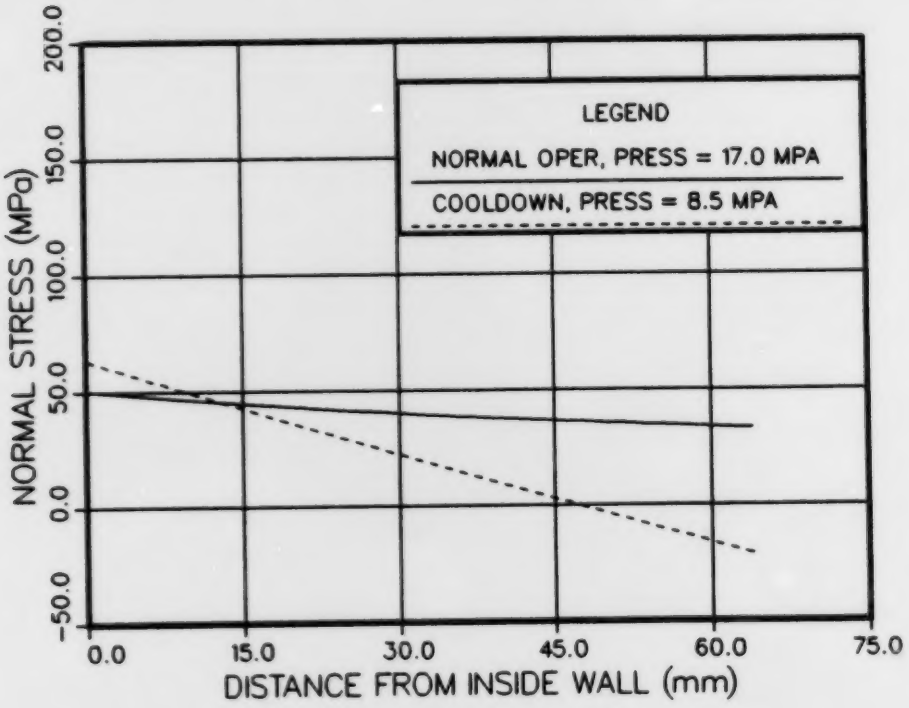

FIGURE 5-5 **Distribution of hoop stress in the discharge valve body with a wall thickness of 64 mm for steady state and cooldown conditions.**

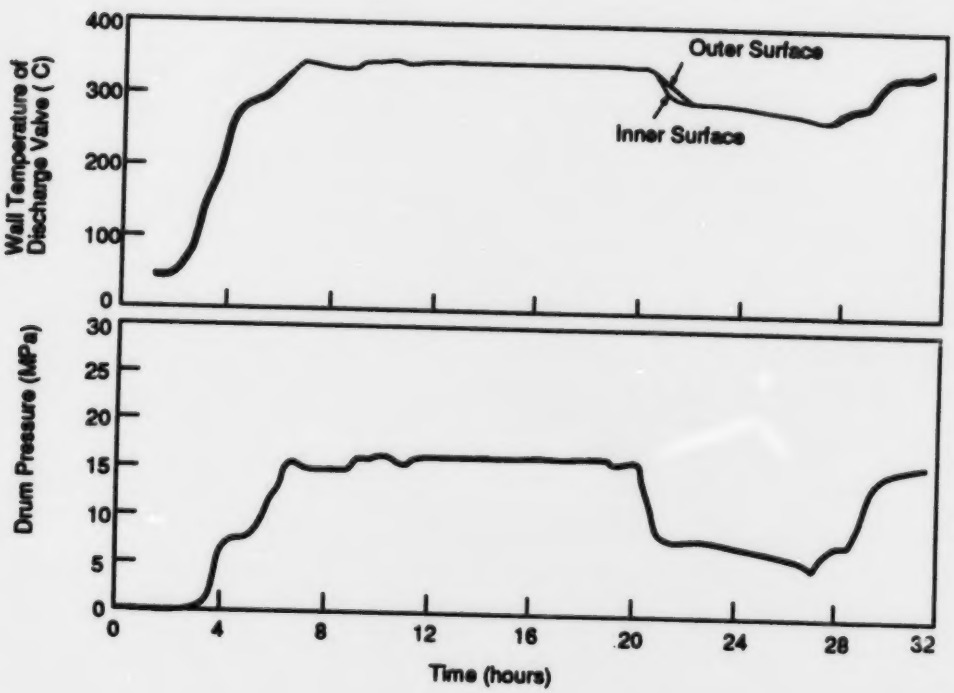

FIGURE 5-6 **Cold start, load changes and shutdown histories for Lambton TGS Unit 2.**

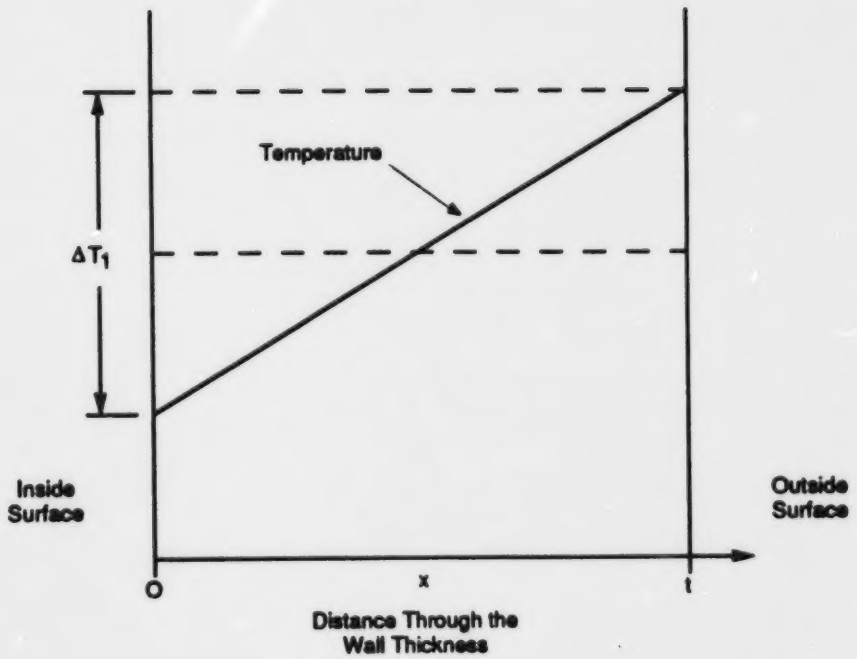

FIGURE 5–7 **Illustration of idealized temperature distribution.**

6.0 CRACK-TIP STRESS INTENSITY FACTORS

The evaluation is based on elastic fracture mechanics with small-scale yielding. Two crack shapes were modelled as illustrated in Figure 6-1. These are a crack with an infinite length/depth aspect ratio, and a semi-elliptical crack with an aspect ratio of 10 to 1. The formulae for the crack-tip stress intensity factor, K_I, correspond to an axial crack in a cylinder, and are given in Appendix B of this report. Formulae for the pump casing are based on the cubic through-wall stress distribution given by equation (5-1). Formulae for the discharge valve body are based on internal pressure in a cylinder, plus a linear through-wall stress distribution to account for the thermal stresses. The formulae for both components account for internal pressure acting on the crack faces.

The calculation of the crack-tip stress intensity factor involved three steps. In the first step K_I is calculated for the actual postulated crack depth a. In the second step a plastic zone size r_y is calculated to account for the plasticity surrounding the crack tip under small-scale yielding conditions. The expression is based on plane-strain conditions and is given by/11/

$$r_y = (1/6\pi)(K_I(a)/\sigma_{ys})^2 \qquad (6\text{-}1)$$

where $K_I(a)$ = the crack-tip stress intensity factor for a crack depth a,
σ_{ys} = the yield stress.

An effective crack depth, a_e, is then calculated from

$$a_e = a + r_y \qquad (6\text{-}2)$$

In the third step the crack-tip stress intensity factor is calculated based on the effective crack depth. In this report the crack depths referenced and plotted in the figures is the actual crack depth, not the effective crack depth.

For the semi-elliptical cracks, K_I is calculated at both the deepest point of crack penetration, and the intersection of the crack front with the inside wall. The maximum value of K_I at the two locations was used. While the plane-strain expression for the plastic zone size is appropriate for the deepest point of penetration, it was not clear what expression was appropriate for the surface intersection point, due to the lack of constraint at the surface. The plastic zone size under plane stress conditions is three times that given by equation (6-1). The procedure employed was to calculate r_y based on the maximum value of K_I at the two points. This value for r_y was used to calculate an effective crack depth by using equation (6-2). The crack aspect ratio was fixed at 10. This implied that the plastic zone size at the surface intersection point was five times the calculated value for r_y, which is considered to be conservative.

The calculations were limited to cases for which the plastic zone size was no more than one-half of the remaining ligament. This was to ensure that elastic small-scale yielding conditions prevailed for the deep cracks.

The safety margin on the crack-tip stress intensity factor is given by the ratio

$$SMK = K_{Ic}/K_I \qquad (6\text{-}3)$$

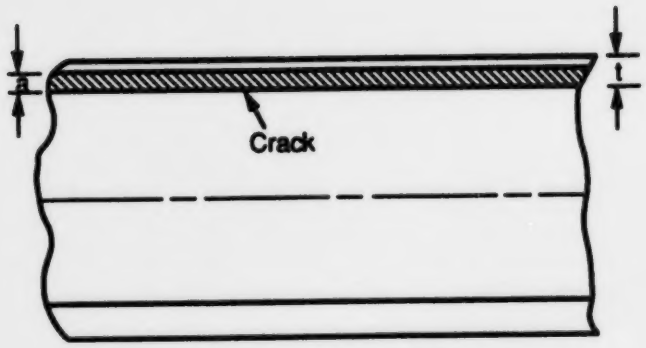

Infinite Aspect Ratio Crack

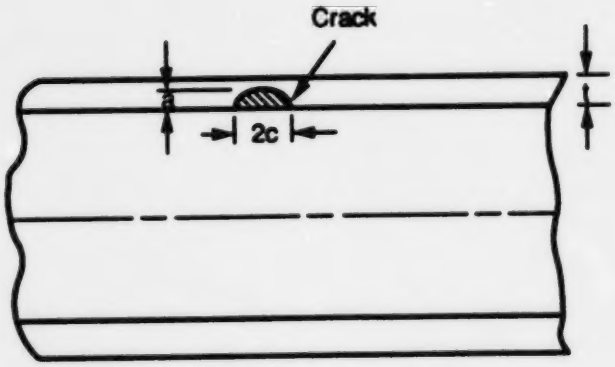

Semi-Elliptical Crack

FIGURE 6-1 Shapes of axial cracks in a cylinder modelled in the evaluation.

7.0 LIMIT LOAD ANALYSIS

Limit load analysis addresses the possibility of failure of the component by plastic collapse of the remaining ligament prior to failure by fracture. Only the primary stresses, which oppose the external forces (in this case internal pressure and dead-weight) are included in the applied loads.

7.1 Limit Load Analysis for the Pump Casing

Following reference /15/, the remote membrane stress at limit load, σ_o, is estimated by using

$$\sigma_o = (2/\sqrt{3})\ \sigma_f\ (1 - (a^*/t)) \qquad (7\text{-}1)$$

where σ_f = the material's flow stress

t = the wall thickness,

a^* = the depth of the "equivalent" crack of infinite aspect ratio given by /15,16/

$$a^* = a(1 - 1/f)/(1 - (a/t)/f) \qquad (7\text{-}2)$$

where

$$f = (1 + 2(c/t)^2)^{0.5} \qquad (7\text{-}3)$$

where a = the actual crack depth,

c = one-half the length of the crack.

These limit load expressions can be used for a semi-elliptical crack, or an infinite aspect ratio crack, in which case $a^* = a$.

The safety margin against plastic collapse is written as

$$SMP = \sigma_o/(\sigma_{prim} + (a/t)p) \qquad (7\text{-}4)$$

where σ_{prim} = the applied primary stress given by equation (5-2),

p = internal pressure.

The stress on the remaining ligament due to pressure acting on the crack faces has been included in equation (7-4).

7.2 Limit Load Analysis for the Discharge Valve Body

The limit pressure, p_o, for an internally pressurized cylinder containing a crack with an infinite aspect ratio is given in reference /11/.

The safety margin against plastic collapse (p_o/p) is given by

$$SMP = (2/\sqrt{3})\ \sigma_f(t-a)/(R_c p) \quad (7\text{–}5)$$

where $R_c = R_i + a$, (7–6)

R_i = the inner wall radius.

8.0 FATIGUE CRACK GROWTH

Following ASME Section XI Appendix A/17/, the Paris Rule was used to predict subcritical crack growth due to fatigue. The fatigue crack growth rate da/dN is given by

$$da/dN = C_1 \Delta K_I^n \quad (8\text{–}1)$$

where ΔK_I = range in the crack-tip stress intensity factor over the load cycle,

$$\Delta K_I = K_{Imax} - K_{Imin}, \quad (8\text{–}2)$$

K_{Imin} = the minimum value of K_I for the cycle,

K_{Imax} = the maximum value of K_I for the cycle,

C_1,n are material property fatigue growth rate parameters which are a function of ΔK_I and the R-ratio, where

$$R = K_{Imin}/K_{Imax}. \quad (8\text{–}3)$$

The value of ΔK_I at a given crack depth "a" was taken to be the maximum of the crack-tip stress intensity factors (calculated by following Section 6) for the normal operating steady-state pressure of 17.0 MPa, and the cooldown transient at a pressure of 8.5 MPa.

Values for the growth rate parameters C_1 and n specific to A216 WCB steel in a water environment were not found. Values for A216 WCC in an air environment were found in reference /18/, and are $C_1 = 2.3 \times 10^{-10}$ and $n = 3.0$ for da/dN in inches/cycle and ΔK_I in ksi $\sqrt{in.}$ This curve is compared with the air environment curve given in ASME Section XI Appendix A in Figure 8–1. The A216 WCC air curve falls just below the ASME air curve. The ASME Section XI curve for a water environment with an R-ratio = 0.0 (see Figure 8–1) was used in this evaluation. This curve is based on light water nuclear reactor environments.

Equation (8–1) was integrated numerically to produce curves of crack depth versus number of cycles. Calculations were performed for both infinite aspect ratio cracks and semi-elliptical cracks with an aspect ratio of 10 to 1. The integration was stopped when the plastic zone size reached one-half of the remaining ligament. The resulting curves are given in Appendix C of this report.

Unit 3 has undergone 800 starts, and has logged 114,000 operating hours. The fatigue crack growth of the shallower cracks after 800 starts is predicted from the curves to be insignificant. The deepest crack found in a pump casing had an aspect ratio of 5.7, was 77% through the wall, and was located in the upper corner region. The initial crack depth would have had to be 70% through the wall to

grow to its final depth in 800 cycles. The deepest crack found in a discharge valve body was 55% through the wall. The initial crack depth would have had to be 50% through the wall to grow to its final depth in 800 cycles. Therefore, the mechanism for the large extent of the growth of these cracks has not been identified. The growth may be due to a corrosion related fatigue mechanism.

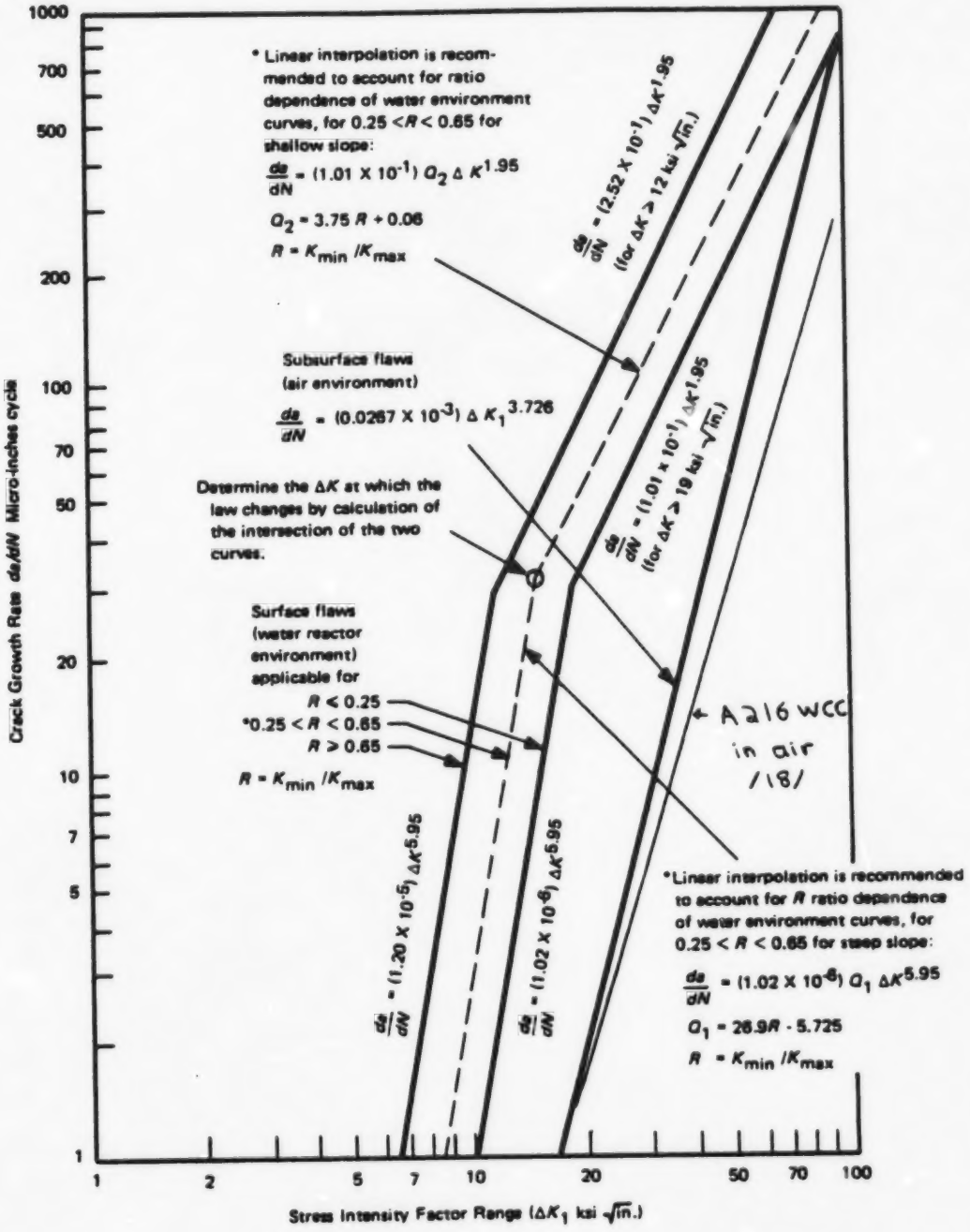
Crack Growth Rate da/dN Micro-inches cycle
1000
700
500
200
100
70
50
20
10
7
5
1
1
2
5
7
10
20
50
70
100
Stress Intensity Factor Range (ΔK1 ksi √in.)
* Linear interpolation is recommended to account for ratio dependence of water environment curves, for 0.25 < R < 0.65 for shallow slope:
da/dN = (1.01 X 10-1) Q2 Δ K1.95
Q2 = 3.75 R + 0.06
R = Kmin /Kmax
Subsurface flaws (air environment)
da/dN = (0.0267 X 10-3) Δ K1 3.726
Determine the ΔK at which the law changes by calculation of the intersection of the two curves.
Surface flaws (water reactor environment) applicable for
R < 0.25
*0.25 < R < 0.65
R > 0.65
R = Kmin /Kmax
da/dN = (2.52 X 10-1) ΔK1.95 (for ΔK > 12 ksi √in.)
da/dN = (1.01 x 10-1) ΔK1.95 (for ΔK > 19 ksi √in.)
da/dN = (1.20 X 10-5) ΔK5.95
da/dN = (1.02 X 10-6) ΔK5.95
A216 WCC in air /18/
*Linear interpolation is recommended to account for R ratio dependence of water environment curves, for 0.25 < R < 0.65 for steep slope:
da/dN = (1.02 X 10-6) Q1 ΔK5.95
Q1 = 26.9R - 5.725
R = Kmin /Kmax

FIGURE 8-1 **Reference fatigue crack growth curves for carbon and low alloy ferritic steels (from Reference /17/).**

9.0 EVALUATION OF SAFETY MARGINS

Safety margins on the crack-tip stress intensity factor (fracture initiation) and on limit load (plastic collapse) were calculated for cracks with an infinite aspect ratio, and for semi-elliptical cracks with an aspect ratio of 10 to 1. The lengths of the deepest semi-elliptical cracks exceeded the size which would physically fit into the component in a reasonable fashion. The crack length would have to be shortened to fit in the component. However, since the severity of the crack increases with length, the aspect ratio of 10 to 1 was used for all crack depths. The safety margins for the valve body are only applicable to cracks which lie in regions in the valve body where the dominant pressure-induced stress field is characterized by equation (5-3). This excludes cracks lying in regions where the stresses are dominated by a three-dimensional stress concentration.

The lowest safety margins of all the operating conditions correspond to the hydrostatic test pressure of 22.0 MPa. These minimum safety margins for the pump casing and discharge valve body are summarized in Tables 9-1 and 9-2, respectively. The locations given in the tables for the 3 mm deep crack in the pump casing and the 10 mm deep crack in the discharge valve body are the "worst case" locations, while the locations given for the deepest cracks detected, and subsequently repaired, are the locations at which the cracks were found. The deepest crack found in a pump casing was 75 mm deep, which was 77% through the 97 mm wall thickness. In this evaluation safety margins were calculated for the 91 mm design minimum wall thickness to obtain upper-bound stresses. The 77% through-wall thickness crack quoted in this evaluation is actually 71 mm deep. The safety margins for the 71 mm deep crack in a 91 mm thick wall will be slightly lower than the margins for a 75 mm deep crack in a 97 mm thick wall.

9.1 Safety Margins on the Crack-Tip Stress Intensity Factor

Safety margins on the crack-tip stress intensity factor were calculated using equation (6-3) as a function of crack depth for each of the following pressure/temperature states:

normal operating	- pressure = 17.0 MPa - temperature = 366°C
cooldown (discharge valve only)	- pressure = 8.5 MPa - temperature = 325°C
operating overpressure	- pressure = 18.0 MPa - temperature = 366°C
minimum safety valve setting	- pressure = 19.7 MPa - temperature = 366°C
hydrostatic test	- pressure = 22.0 MPa - temperature = 25°C
1.4 x normal operating pressure	- pressure = 23.8 MPa - temperature = 366°C

The highest pressure the components would be subjected to would be the hydrostatic test pressure of 22.0 MPa.

From Section 6.0, the effects of small-scale plasticity at the crack tip means that the safety margin on the crack-tip stress intensity factor is not linearly proportional to pressure. The pressure of 1.4 times normal operating pressure was chosen to predict the crack depth at which a margin of at least 1.4 on pressure would exist.

9.1.1 Safety Margins for the Pump Casing

The curves of safety margin as a function of crack depth for Profile 1 for the infinite aspect ratio and semi-elliptical cracks are given in Figures 9-1 and 9-2, respectively. The corresponding curves for Profile 2 are given in Figures 9-3 and 9-4. The deepest cracks left in the pump casings were 3 mm deep. The safety margins for the 3 mm deep cracks for pressures up to the hydrostatic test pressure are greater than 4.0. The crack-tip stress intensity factor for the semi-elliptical cracks for Profile 1 at the surface intersection point became greater than that at the deepest point of crack penetration for crack depths greater than 55 mm. The corresponding depth for Profile 2 was 65 mm. This is due to the strong through-wall bending stresses. See Figures 5-2 and 5-3.

The deepest crack found was in pump B in the upper corner region, and was 77% through the wall thickness. The aspect ratio was 5.7, rather than the slightly more severe aspect ratio of 10 modelled in this evaluation. The margin on the crack-tip stress intensity factor for this crack at the normal operating pressure of 17.0 MPa was predicted to be 1.82, and for the hydrostatic test pressure of 22.0 MPa to be 1.42. At the operating temperature of 366°C ductile material fracture behaviour is ensured. The margin at 366°C represents the margin against ductile crack initiation. The margin against failure of the pump casing is expected to be slightly higher.

9.1.2 Safety Margins for the Discharge Valve Body

The curves of safety margin as a function of crack depth for the 47 mm wall thickness valve body for the infinite aspect ratio crack and semi-elliptical cracks are given in Figures 9-5 and 9-6, respectively. The corresponding curves for the 64 mm wall thickness valve body are given in Figures 9-7 and 9-8. The crack-tip stress intensity factor of the semi-elliptical crack was always greater at the deepest point of crack penetration compared with the surface intersection point.

The deepest cracks left in the valve bodies are 10 mm deep. The safety margins for the 10 mm deep cracks for pressures up to the hydrostatic test pressure are greater than 5.0.

The deepest crack found in a discharge valve body was 55% through the wall thickness. The margin for an infinite aspect ratio crack 55% through the 64 mm wall thickness (lowest wall thickness measured) at the normal operating pressure was predicted to be 2.89, and at the hydrostatic test pressure to be 2.26.

9.2 Safety Margins Against Plastic Collapse

The safety margins against plastic collapse were calculated as a function of crack depth for the pump casing as outlined in Section 7.1, and for the discharge valve body as outlined in Section 7.2. The load states are the same as were used to calculate the margins on the crack-tip stress intensity factor.

9.2.1 Safety Margins for the Pump Casing

The safety margins for Profile 2 were lower than those for Profile 1, and only the results for Profile 2 are given in this report. The curves of safety margin as a function of crack depth for Profile 2 for an infinite aspect ratio crack are given in Figure 9-9, and for an aspect ratio of 10 in Figure 9-10. The safety margins for the deepest cracks left in the pump casings (3 mm) for pressures up to the hydrostatic test pressure are greater than 6.0. The margin for the semi-elliptical crack at a depth of 77% of the wall thickness is 1.68 for the normal operating pressure, and 1.43 for the hydrostatic test pressure.

9.2.2 Safety Margins for the Discharge Valve Body

The curves of safety margin as a function of crack depth for an infinite aspect ratio crack in the 47 mm wall thickness valve body are given in Figure 9-11, and in the 64 mm wall thickness valve body in Figure 9-12. The safety margins for the deepest cracks left in the valve bodies (10 mm) for pressures up to the hydrostatic test pressure are greater than 4.0. The margin for a crack depth of 55% of the 64 mm wall thickness is 3.48 for the normal operating pressure, and 2.97 for the hydrostatic test pressure.

9.3 Recommendations

a) The detected cracks which remain in the boiler circulation pump casings and discharge valve bodies of Lambton TGS Unit 3 are acceptable for continued service.

b) The circulation pumps and discharge valves in all the units in the Lambton TGS should be periodically subjected to a hydrostatic test at a pressure of 22.0 MPa.

c) The circulation pumps and discharge valves in all the units in the Lambton TGS should be subjected to a periodic inspection.

d) The cause of the extent of the subcritical crack growth should be identified.

10.0 ACKNOWLEDGEMENTS

The author wishes to acknowledge the assistance of Mr. R.L. McQueen, Mr. D.D. McNabb and Dr. D. Sidey of the Chemistry and Metallurgy Department of CTS, along with Mr. N. Rowed of the Lambton TGS. The author also acknowledges the efforts of Mr. O.E. Lepik, Mr. D.W. Carpenter and Mr. D.M. McCluskey of the Fracture Mechanics Unit for carrying out the A216 WCB fracture toughness tests under severe time constraints.

Approved:

J. Brown
Manager
Metallurgical Research Dept

Prepared:

D.A. Scarth
Engineer
Nondestructive and Fracture Evaluation Section

Recommended:

B. Mukherjee
Acting Section Head
Nondestructive and Fracture Evaluation Section

DAS:SEHG

REFERENCES

1. McNabb, D.D., "Lambton TGS Boiler Circulation Pump Discharge Valve Crack Analysis", Chemistry and Metallurgy Dept., Central Thermal Services, Report No. CTS-31130-9, May 6, 1987.

2. ASME Boiler and Pressure Vessel Code, Section III, Division 1, Appendix I, 1980.

3. ASME Boiler and Pressure Vessel Code, Section II, Part A, 1983.

4. "Report of Chemical Analysis - Recirculating Pump Casing U-3 from Lambton", Chemical Research Department Report No. CE-88-4688-K, August 29, 1988.

5. "Report of Chemical Analysis - Boiler Valve Sample, Lambton TGS - U3", Chemical Research Department Report No. CE-88-3953-K, July 30, 1988.

6. Lepik, O.E., McCluskey, D.M. and Carpenter, D.W., "Fracture Toughness Properties of A216 Gr WCB Cast Steel", Metallurgical Research Department, draft report no. 88-195-K.

7. "Standard Test Method for Determining J_{Ic}, a Measure of Fracture Toughness", ASTM Standard E813-87, Vol. 03.01, 1987, pp. 968-990.

8. Barnby, J.T. and al-Daimalani, I.S., "Assessment of the Fracture Toughness of Cast Steels", Journal of Materials Science, 1976, pp. 1989-1994.

9. "ABAQUS User's Manual", Version 4.6, Hibbitt, Karlsson and Sorenson, Inc., Providence, Rhode Island, 1987.

10. Timoshenko, S.P. and Goodier, J.N., "Theory of Elasticity", Third Edition, McGraw-Hill, 1970.

11. Kumar, V., German, M.D. and Shih, C.F., "An Engineering Approach for Elastic-Plastic Fracture Analysis", EPRI Report NP-1931, July, 1981.

12. Buchalet, C.B. and Bamford, W.H., "Stress Intensity Factor Solutions for Continuous Surface Flaws in Reactor Pressure Vessels", ASTM STP 590, 1976, pp. 385-402.

13. Raju, I.S. and Newman, J.C., "Stress Intensity Factors for Internal and External Surface Cracks in Cylindrical Vessels", ASME Journal of Pressure Vessel Technology, Vol. 104, November 1982, pp. 293-298.

14. Rooke, D.P. and Cartwright, D.J., "Compendium of Stress Intensity Factors", Her Majesty's Stationary Office, London, 1976.

15. Miller, A.G., "Review of Limit Loads of Structures Containing Defects", CEGB Report No. TPRD/B/0090/N82, Central Electricity Generating Board, Berkley Nuclear Laboratories, April, 1987.

16. Chell, G.G., "Elastic-Plastic Fracture Mechanics", Chapter 3 in "Developments in Fracture Mechanics-1", G.G. Chell editor, Applied Science, 1979.

17. ASME Boiler and Pressure Vessel Code, Section XI, 1987.

18. Clark, W.G. and Wessel, E.T., "Application of Fracture Mechanics Technology to Medium-Strength Steels", ASTM STP 463, 1970, pp. 160-190.

TABLE 9-1

Minimum Safety Margins for the Boiler Circulation Pump Casings, Based on the Hydrostatic Test Pressure of 22.0 MPa

Crack Description	Crack Depth (mm)	Margin on Fracture Initiation		Margin on Plastic Collapse	
		Margin	Location	Margin	Location
Deepest Crack Detected and Not Repaired					
Crack Length/Depth Aspect Ratio:					
Infinite -	3	4.58	Profile 1	6.70	Profile 2
10 to 1 -	3	5.17	Profile 1	7.01	Profile 2
Deepest Crack Detected and Repaired					
Crack Length/Depth Aspect Ratio:					
10 to 1 -	71[+]	1.42	Profile 1[++]	1.43	Profile 2

[+]Crack depth was 77% through the wall thickness.
[++]Location where crack was found.

TABLE 9-2

Minimum Safety Margins for the Boiler Circulation Pump Discharge Valve Bodies, Based on the Hydrostatic Test Pressure of 22.0 MPa

Crack Description	Crack Depth (mm)	Margin on Fracture Initiation		Margin on Plastic Collapse	
		Margin	Wall Thickness (mm)	Margin	Wall Thickness (mm)
Deepest Crack Detected and Not Repaired					
Crack Length/Depth Aspect Ratio:					
Infinite –	10	5.24	47	4.34	47
10 to 1 –	10	6.13	47	–	–
Deepest Crack Detected and Repaired					
Crack Length/Depth Aspect Ratio:					
Infinite –	35[+]	2.26	64[++]	2.97	64[++]
10 to 1 –	35[+]	3.14	64[++]	–	–

[+]Crack depth was 55% through the wall thickness.
[++]Wall thickness where crack was found.

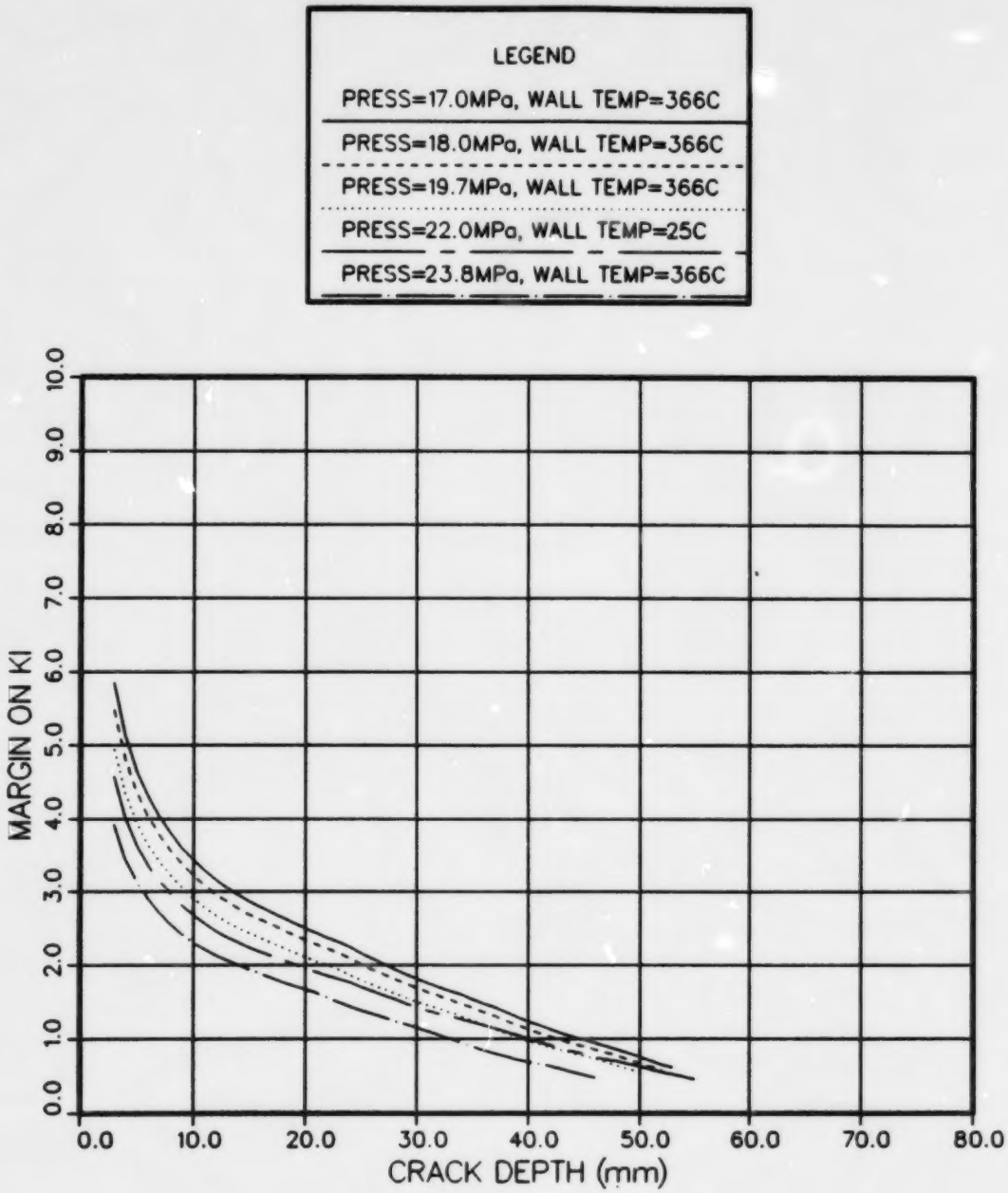

FIGURE 9-1 **Variation of the margin on the crack-tip stress intensity factor with crack depth for a crack with an infinite crack aspect ratio at Profile 1 in the pump casing.**

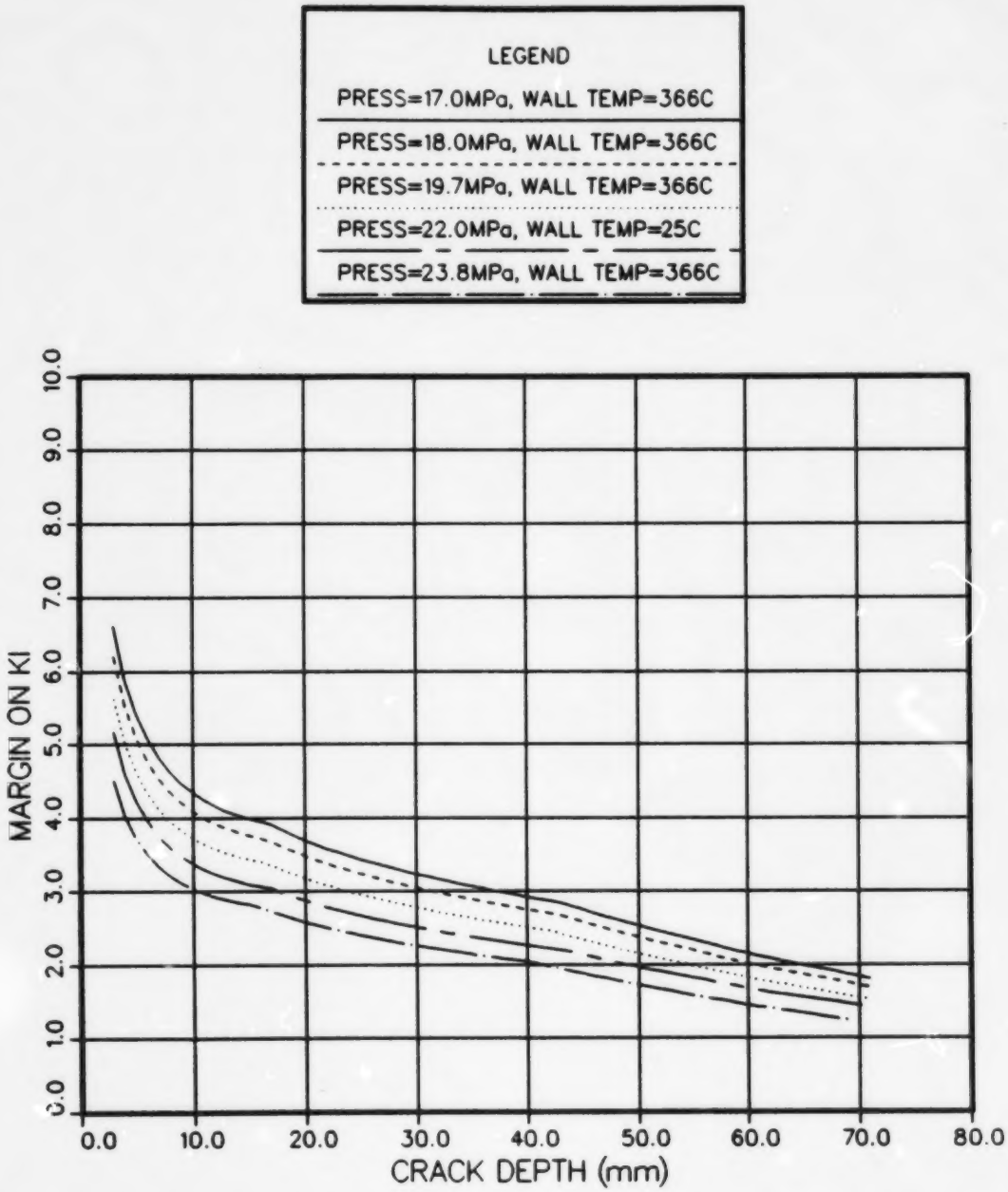

FIGURE 9-2 **Variation of the margin on the crack-tip stress intensity factor with crack depth for a crack with a crack aspect ratio of 10 to 1 at Profile 1 in the pump casing.**

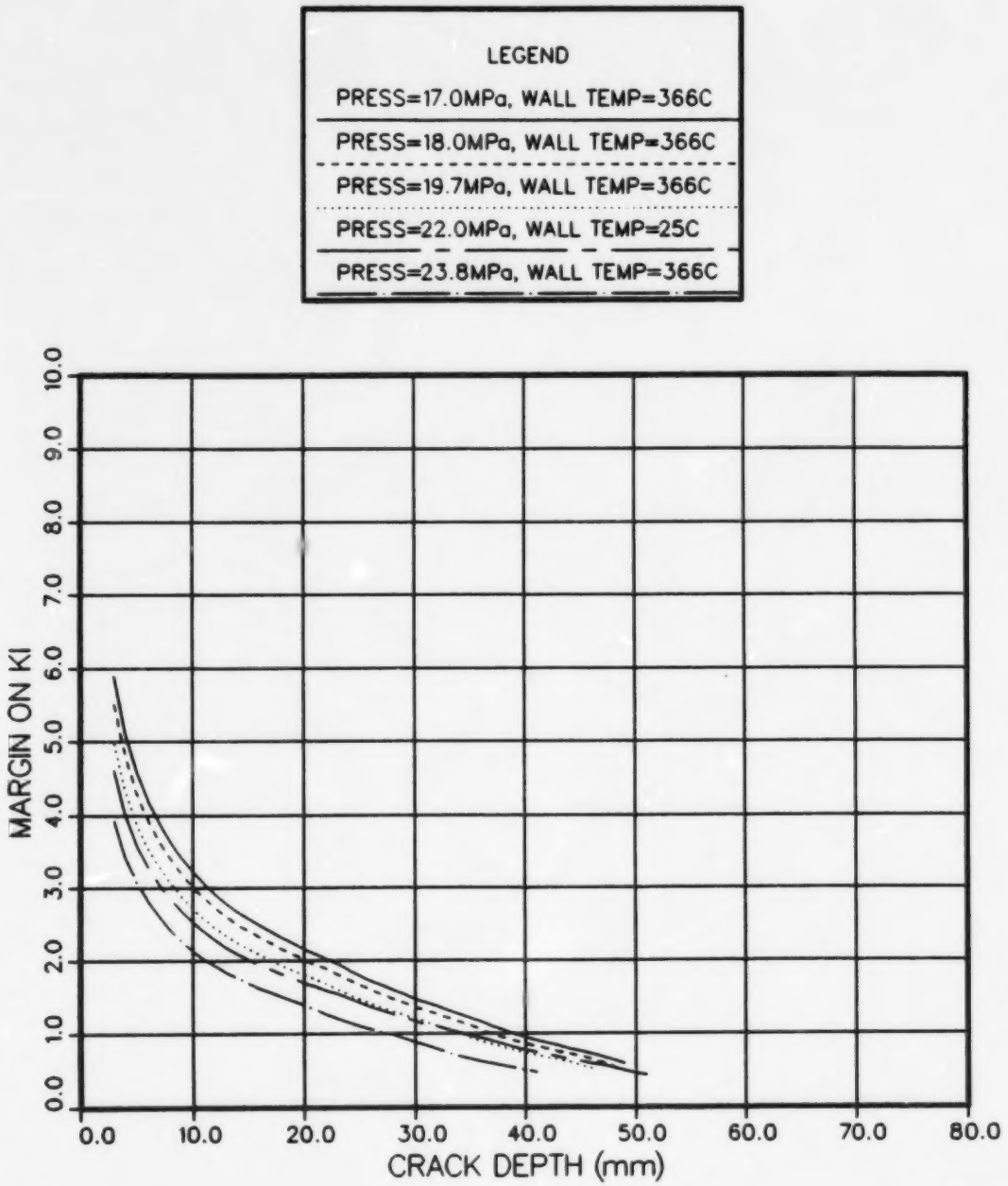

FIGURE 9-3 **Variation of the margin on the crack-tip stress intensity factor with crack depth for a crack with an infinite crack aspect ratio at Profile 2 in the pump casing.**

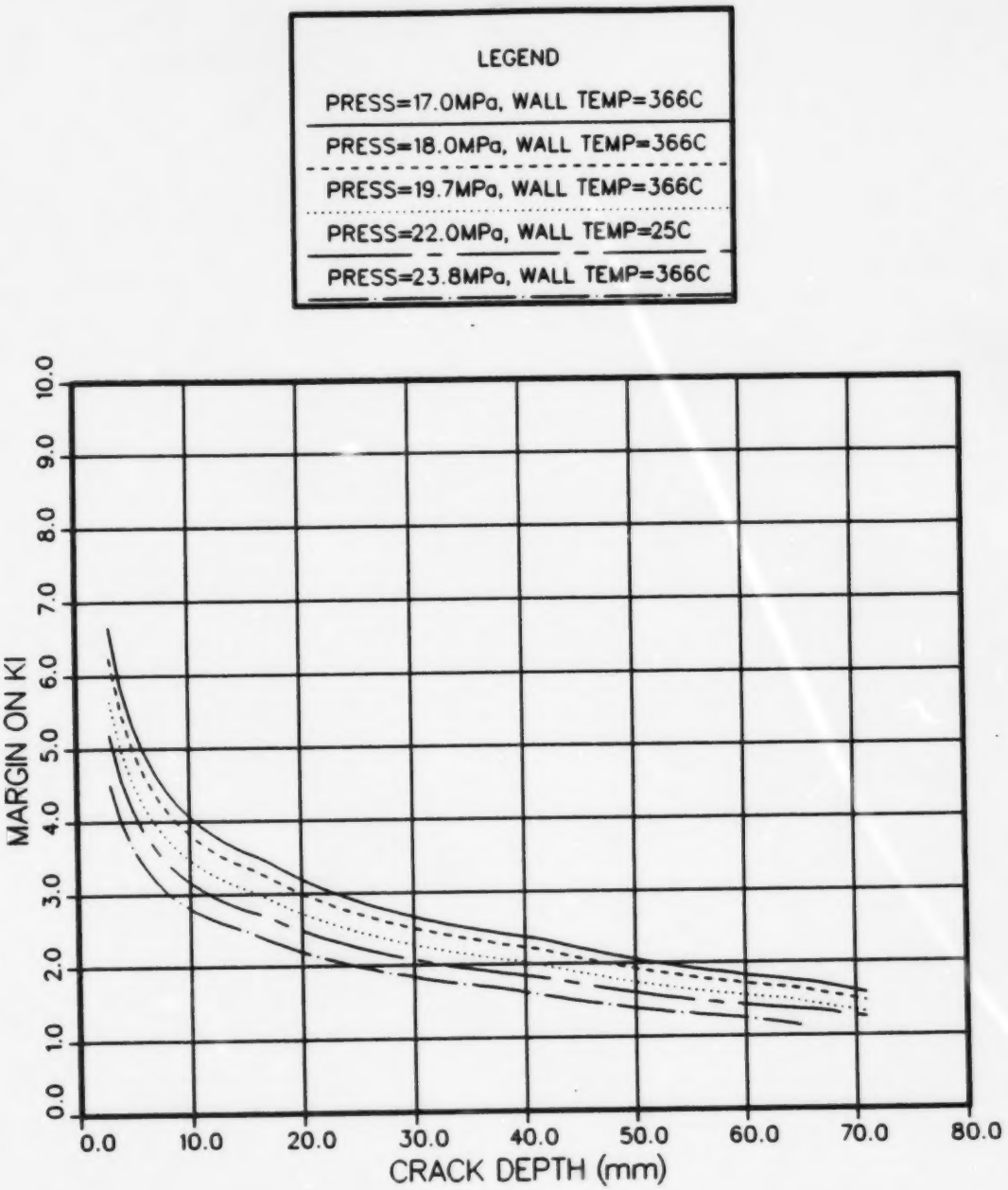

FIGURE 9-4 **Variation of the margin on the crack-tip stress intensity factor with crack depth for a crack with a crack aspect ratio of 10 to 1 at Profile 2 in the pump casing.**

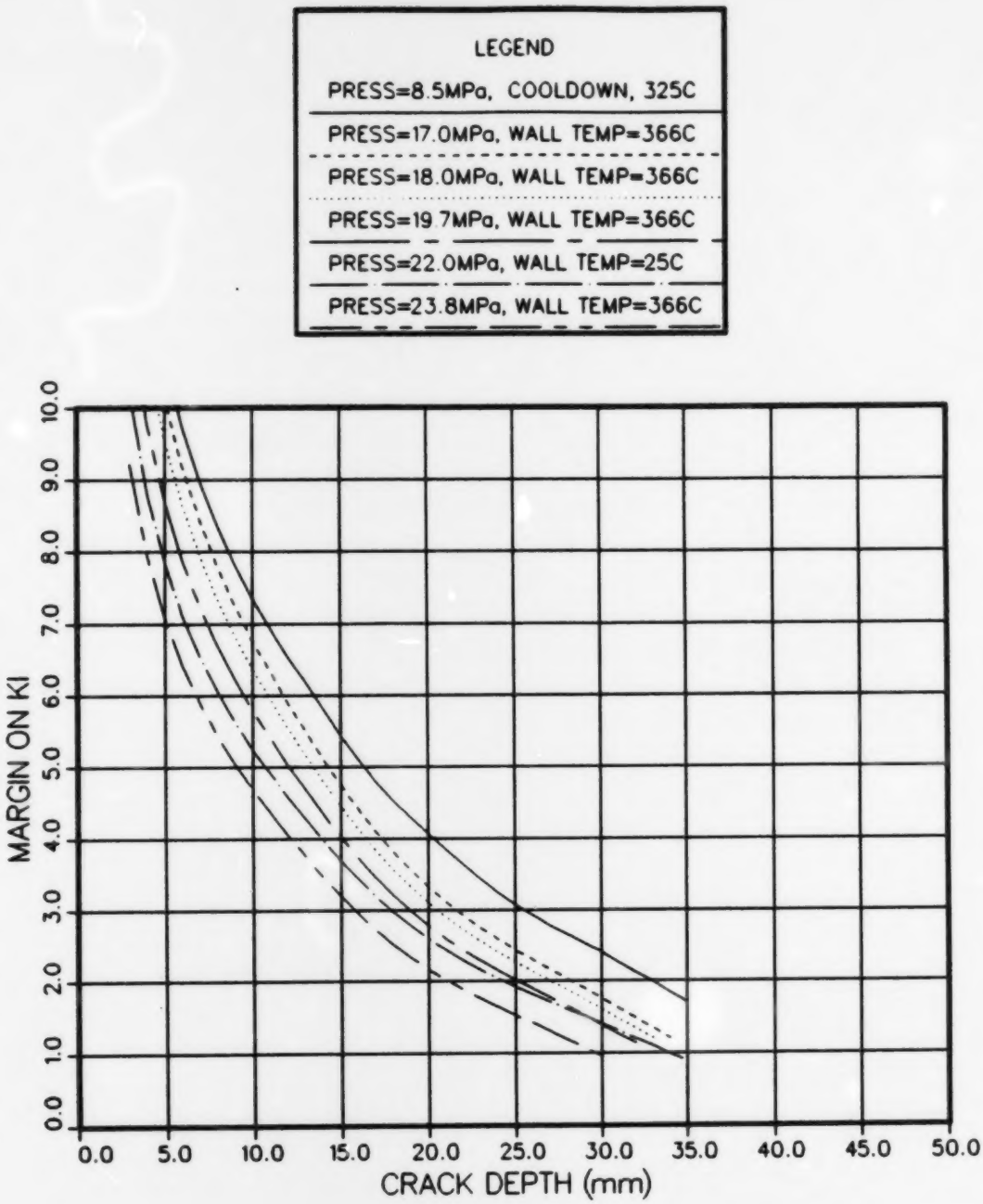

FIGURE 9-5 **Variation of the margin on the crack-tip stress intensity factor with crack depth for a crack with an infinite crack aspect ratio in a discharge valve body with a wall thickness of 47 mm.**

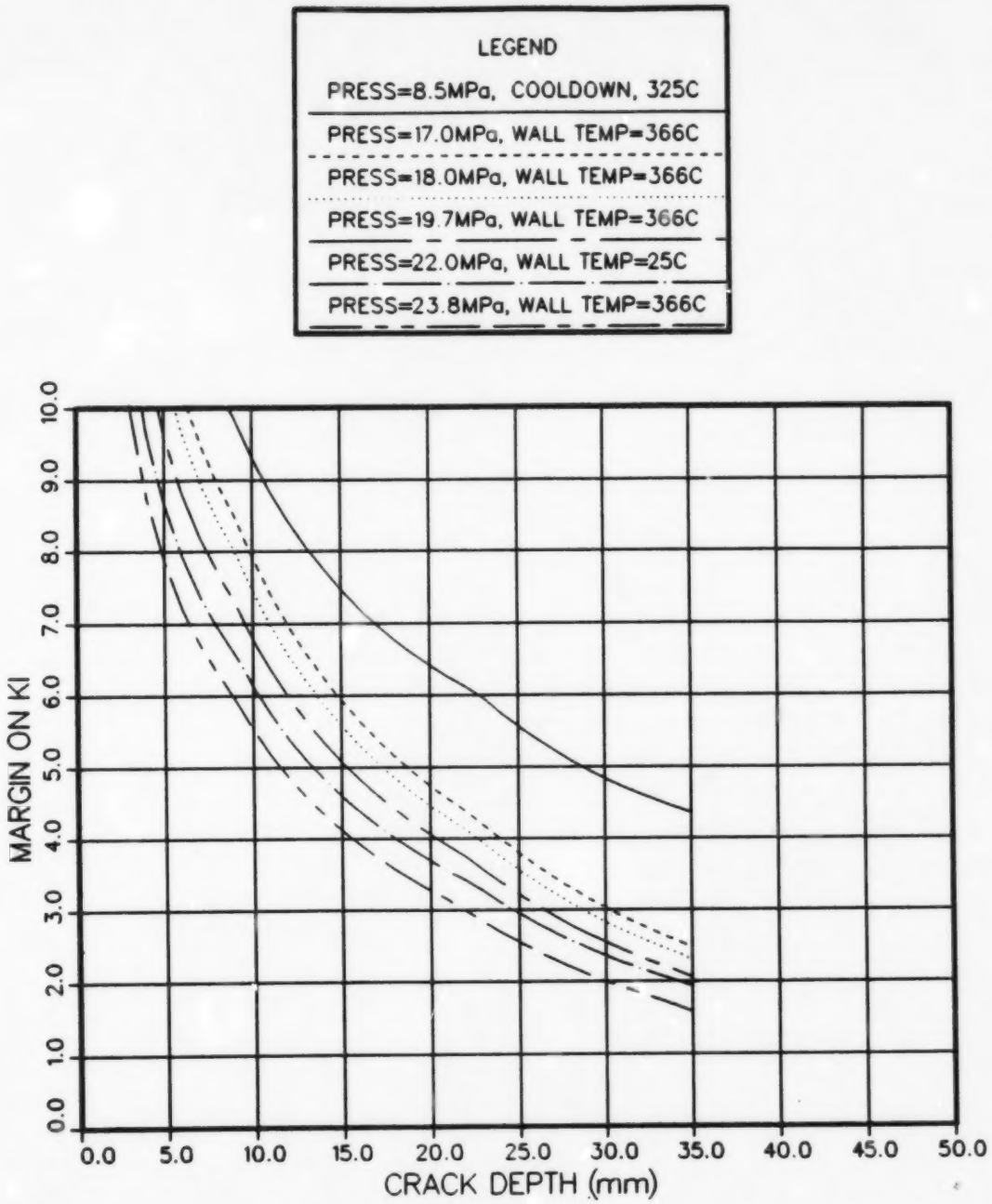

FIGURE 9-6 **Variation of the margin on the crack-tip stress intensity factor with crack depth for a crack with a crack aspect ratio of 10 to 1 in a discharge valve body with a wall thickness of 47 mm.**

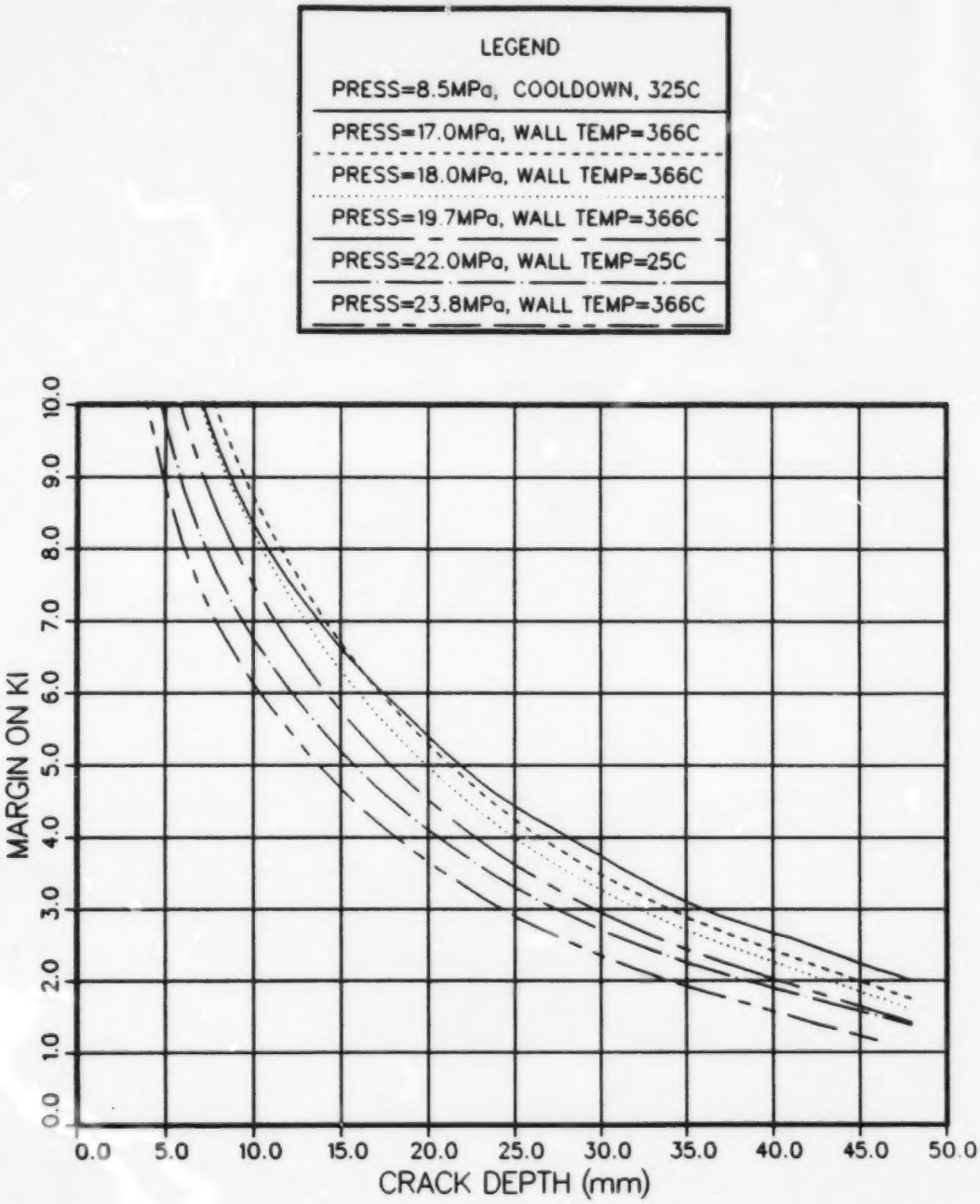

FIGURE 9–7 **Variation of the margin on the crack-tip stress intensity factor with crack depth for a crack with an infinite crack aspect ratio in a discharge valve body with a wall thickness of 64 mm.**

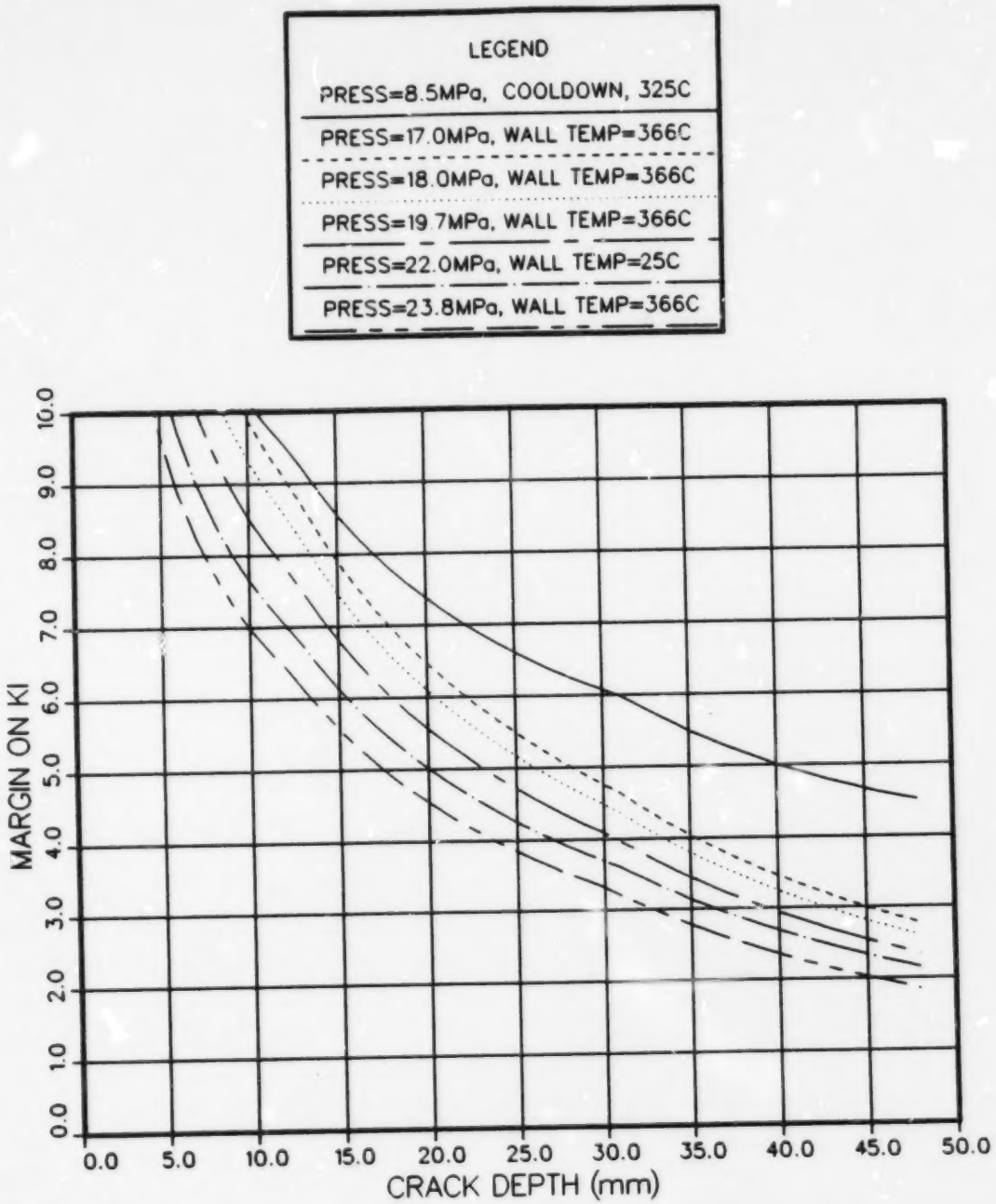

FIGURE 9-8 **Variation of the margin on the crack-tip stress intensity factor with crack depth for a crack with a crack aspect ratio of 10 to 1 in a discharge valve body with a wall thickness of 64 mm.**

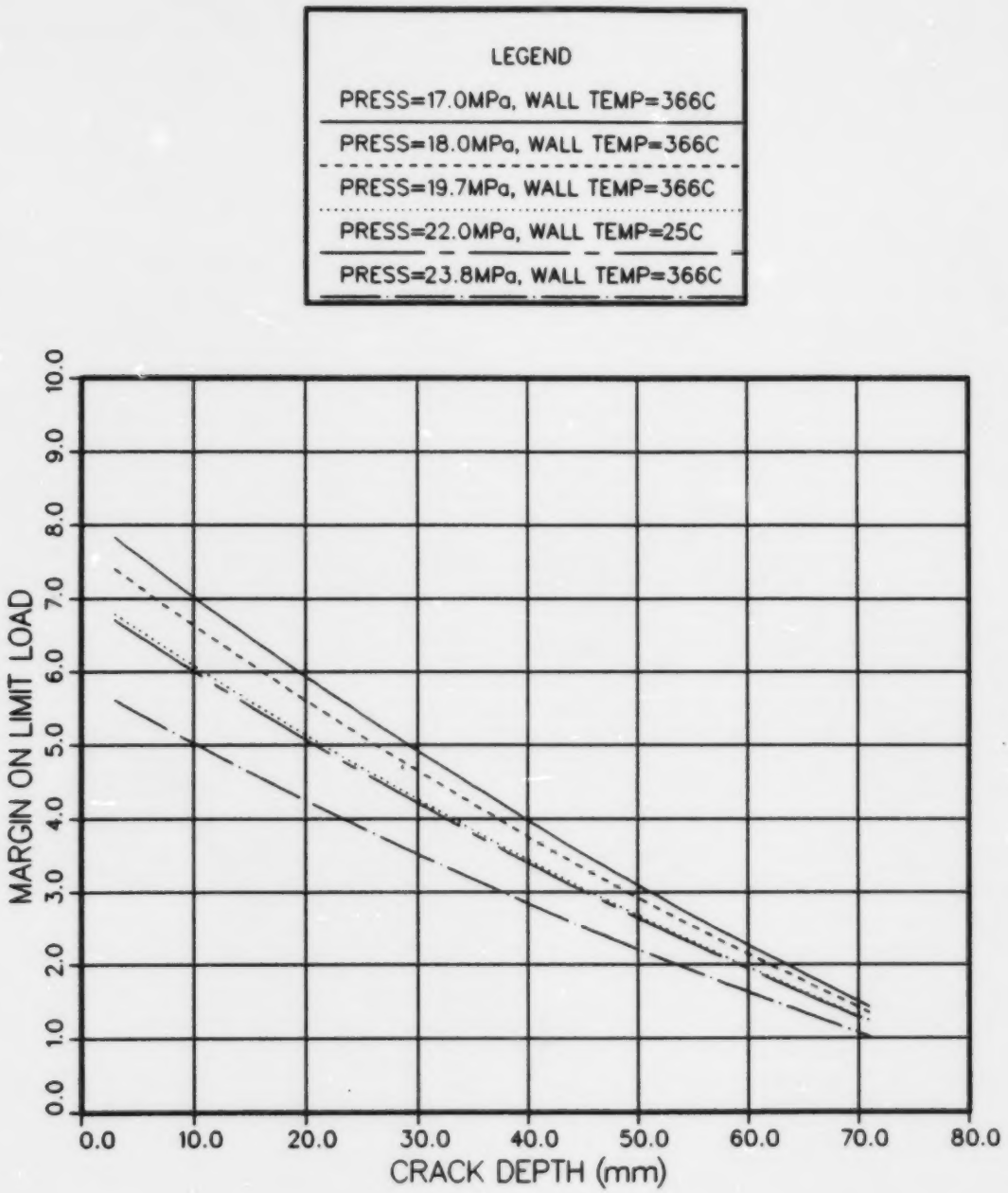

FIGURE 9-9 **Variation of the margin against plastic collapse with crack depth for a crack with an infinite aspect ratio at Profile 2 in the pump casing.**

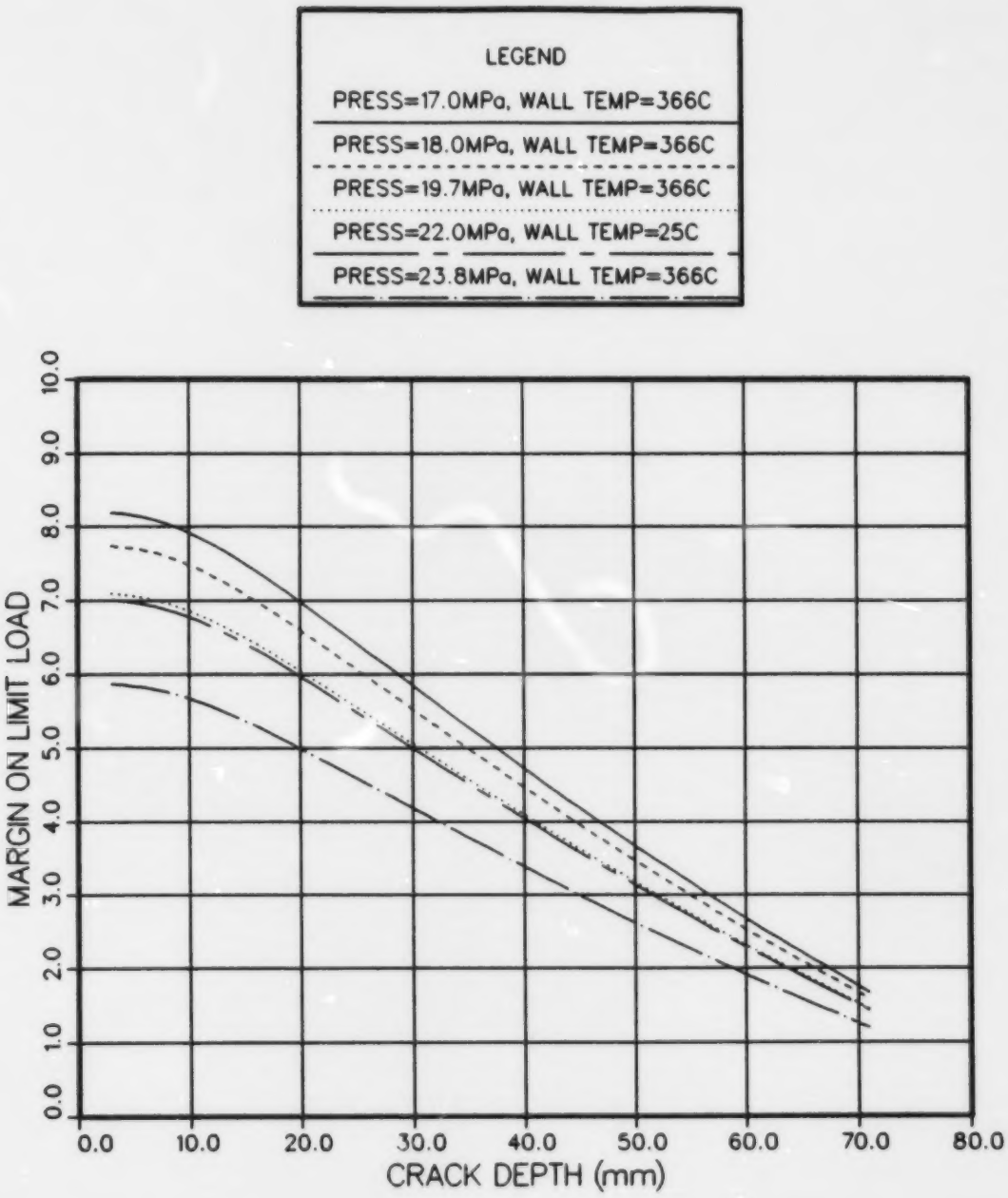

FIGURE 9-10 **Variation of the margin against plastic collapse with crack depth for a crack with an aspect ratio of 10 to 1 at Profile 2 in the pump casing.**

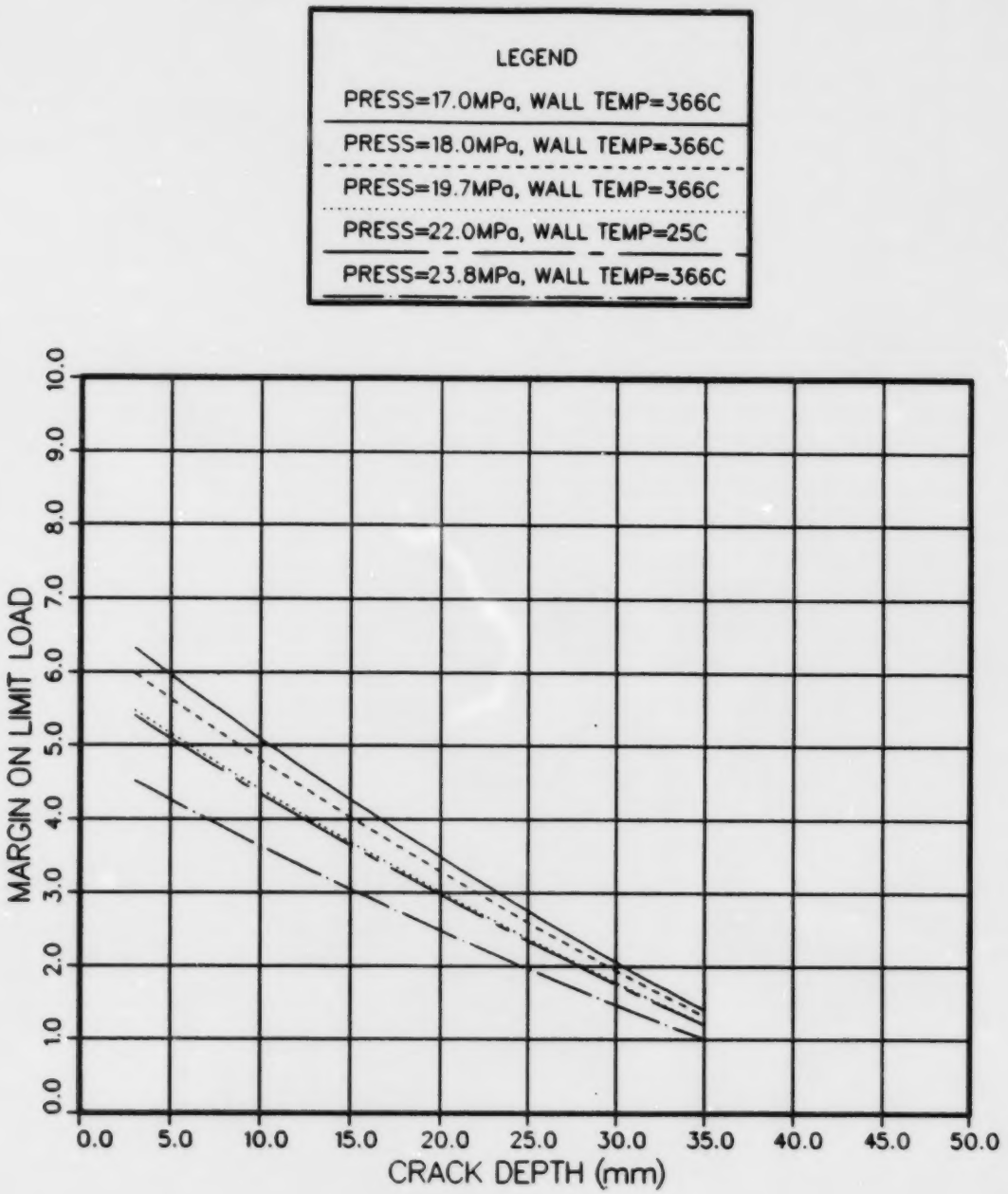

FIGURE 9-11 **Variation of the margin against plastic collapse with crack depth for a crack with an infinite aspect ratio in a discharge valve body with a wall thickness of 47 mm.**

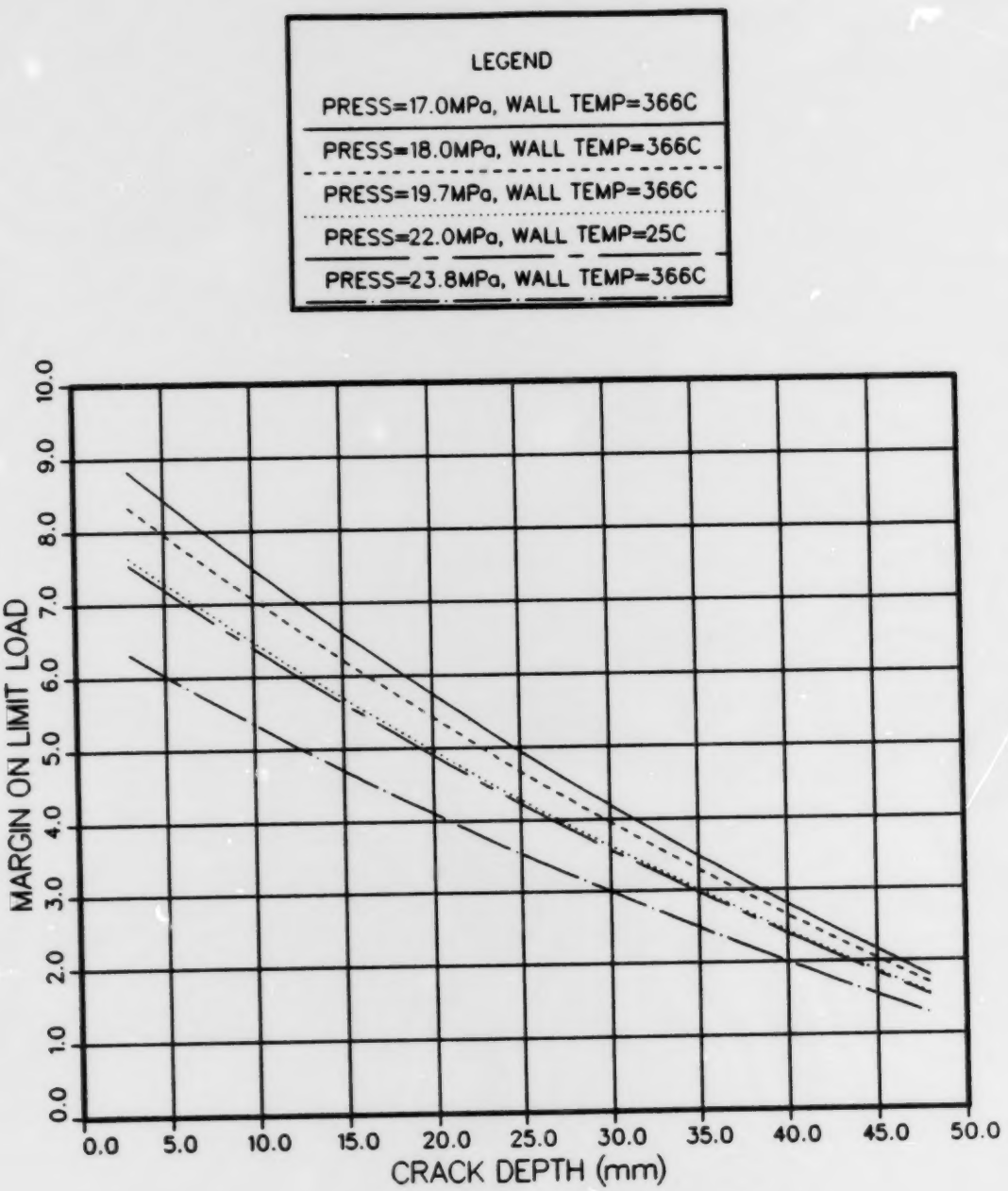

FIGURE 9–12 **Variation of the margin against plastic collapse with crack depth for a crack with an infinite aspect ratio in a discharge valve body with a wall thickness of 64 mm.**

APPENDIX A

Details of the Calculation of Mechanical Stresses in the Pump Casing

A.1 Pump Geometry

The general geometry of the pump casing is illustrated in Figures 1-2 and 1-3. The pump is a single suction - double discharge centrifugal pump. Due to time constraints the three-dimensional pump casing was idealized as two-dimensional axisymmetric. The radii varied with the particular profile chosen in the radial-vertical plane. Two profiles in the radial-vertical plane were selected for the purpose of calculating stresses. Referring to Figure 1-3, these are denoted as Profile 1 and Profile 2. The dimensions of Profile 1 were taken from the Hayward Tyler (manufacturer) drawing no. 39689/G/2 (Ontario Hydro drawing no. NA27-FMG 31130-3) and are given in Figure 5-1. The dimensions of Profile 2 were taken from the same drawing and from field measurements, and are also given in Figure 5-1. Each profile was idealized as the cross-section of an axisymmetric model. Profile 2 is at a larger radius than Profile 1.

The web of the cut water at the discharge (Profile 2) was not included in the axisymmetric idealization. This web carries a portion of the axial load acting on the pump casing and reduces the stresses in the outer wall at the discharge. Therefore, the exclusion of the cut water web should result in upper-bound stresses being calculated in the outer wall.

A.2 Loads

The loads on the pump casing act in the following modes:

a) Internal pressure acting on the inside wall of the pump casing.

b) Axial forces acting on the casing due to the reaction of the suction valve and motor casing to the internal pressure. By treating the top and bottom openings of the pump casing as closed ends, the axial stress on the suction nozzle end due to the internal pressure p is given by

$$S_p = p/((R_{so}/R_{si})^2 - 1.0) \qquad \text{(A-1)}$$

where R_{si} = the inner wall radius of the suction nozzle,

R_{so} = the outer wall radius of the suction nozzle. See Figure 5-1.

c) Axial force due to the weight of the suspended motor. The axial stress on the suction nozzle end is given by

$$S_w = W/(\pi(R_{so}^2 - R_{si}^2)) \qquad \text{(A-2)}$$

where W = the weight of the pump motor,
= 100,000 N.

A.3 Method of Superposition of Stresses

The stresses due to the combined modes of loading are calculated by using linear superposition. This is illustrated in Figure A-1. The actual loading condition is a, which can be expressed in terms of the internal pressure loading on the open casing (condition b) and the axial force on the casing (condition c). The reaction F_3 for

condition b is equal to $p\pi(R_{si}^2 - R_{di}^2)$. Stresses in the casing are calculated (by finite element analysis) for a unit application of internal pressure p for condition b, and for a unit application of axial force F_1 for condition c. The unit stress profiles were fit by using least squares to the cubic equations

$$\sigma_p(x)/p = \tilde{A}_{po} + \tilde{A}_{p1}x + \tilde{A}_{p2}x^2 + \tilde{A}_{p3}x^3 \qquad (A-3)$$

$$\sigma_T(x)/S = \tilde{A}_{To} + \tilde{A}_{T1}x + \tilde{A}_{T2}x^2 + \tilde{A}_{T3}x^3 \qquad (A-4)$$

where $\sigma_p(x)$ = the normal stress distribution due to the internal pressure p acting on the opening casing (condition b),

$\sigma_T(x)$ = the normal stress distribution due to the stress S acting on the suction end of the pump casing (condition c)

$S = F_1/(\pi(R_{so}^2 - R_{si}^2))$ (A-5)

$\tilde{A}_{pi}$ = nondimensional stress coefficients for loading condition b,

$\tilde{A}_{Ti}$ = nondimensional stress coefficients for loading condition c,

x = distance from the inside wall,

t = wall thickness.

For pressure loading on the closed-ended casing, the required force F_2 in condition a will be equal to the closed-ended force F_1 for condition c minus the magnitude of the reaction force for the open vessel condition b.

$$F_2 = F_1 - |F_3| \qquad (A-6)$$

Therefore, for any given internal pressure, the axial force boundary condition of condition a is met by summing the load states of conditions b and c.

The axial stress on the suction nozzle due to the closed-end pressure force is given by equation (A-1). Upon combining equations (A-1) to (A-6) the coefficients A_i in equation (5-1) of Section 5.1 due to the internal pressure p and motor weight W are given by

$$A_i = p[\tilde{A}_{pi} + \tilde{A}_{Ti}/((R_{so}/R_{si})^2 - 1.0) + W\tilde{A}_{Ti}/(\pi(R_{so}^2 - R_{si}^2)) \qquad (A-7)$$

A.4 Finite Element Stress Analysis

The stresses in the uncracked component where calculated by using linear elastic axisymmetric finite element analysis. The finite element computer code was ABAQUS Version 4.6-171/9/, and the element type was the 8-noded isoparametric axisymmetric element with full 9-point Gauss integration. Finite element models were constructed for Profile 1 and Profile 2, and are given in Figures A-2 and A-3, respectively. The model of Profile 1 consists of 318 elements and 1095 nodes, while Profile 2 consists of 369 elements with 1266 nodes. As mentioned in Section A-1, neglecting the cut water web at the discharge should result in upper-bound stresses in Profile 2.

Two runs were performed for each profile model. The first run consisted of the loading condition b in Figure A-1, in which the internal pressure was applied to the entire inside surface from the top of the suction nozzle to the bottom of the motor flange. The vertical displacements of the bottom of the model were fixed to react to the pressure-induced force imbalance. The second run consisted of loading condition c, in which a uniform axial stress was applied to the top of the suction nozzle. The bottom of the motor flange was again fixed to react to the axial force.

The stress required for the fracture mechanics assessment is the normal stress acting perpendicular to the crack. Since the cracks are assumed to lie perpendicular to the inside wall surface of the pump casing, the stress acting perpendicular to the normal vector to the inside surface is required. Denoting the surface normal vector as $\bar{n}$, the normal stress on the crack plane, $\sigma_p(x)$ (or $\sigma_T(x)$), is given by the transformation

$$\sigma_p(x) = \bar{n} \cdot \bar{\bar{\sigma}}\, \bar{n} \qquad \text{(A-8)}$$

where $\bar{\bar{\sigma}}$ is the stress tensor in the cylindrical (r, z,θ) coordinate system and "·" denotes the vector inner product. In the present case equation (A-8) can be written as

$$\sigma_p(x) = n_r^2\, \sigma_{rr} + 2\, n_r n_z\, \sigma_{rz} + n_z^2\, \sigma_{zz} \qquad \text{(A-9)}$$

A.5 Stress Results

The through-wall distributions of normal stress were plotted for several locations around the "C" section of the volute. The most severe stress distribution for each profile was used in the evaluation. This corresponded to the upper corner region for Profile 1, and the midsection for Profile 2. The stress distribution for load condition b, normalized by dividing by the internal pressure, for Profile 1 at the upper corner region is given in Figure A-4, and the stress distribution for load condition c, normalized by dividing by the remote stress on the suction end, is given in Figure A-5. Also shown on each plot is the least-squares fit of equations (A-3) and (A-4) to the finite element results. The corresponding plots for Profile 2 at the midsection are given in Figures (A-6) and (A-7), respectively. The nondimensional coefficients $\tilde{A}_{pi}$ and $\tilde{A}_{Ti}$ from the least-squares fit of equations (A-3) and (A-4) for Profile 1 – upper corner and Profile 2 – midsection are given in Table A-1.

TABLE A-1

Normalized Normal Stress Coefficients for the
Cubic Stress Distribution for the Pump Casing

Coefficient	Profile 1 – Upper Corner	Profile 2 – Midsection
$\tilde{A}_{po}$	65.352	68.078
$\tilde{A}_{p1}$	-2554.3	-1493.7
$\tilde{A}_{p2}$	38,829	10,504
$\tilde{A}_{p3}$	-209,236	-42,354
$\tilde{A}_{T0}$	22.744	17.839
$\tilde{A}_{T1}$	-884.97	-428.98
$\tilde{A}_{T2}$	12,714	2655.6
$\tilde{A}_{T3}$	-65,382	-9516.0

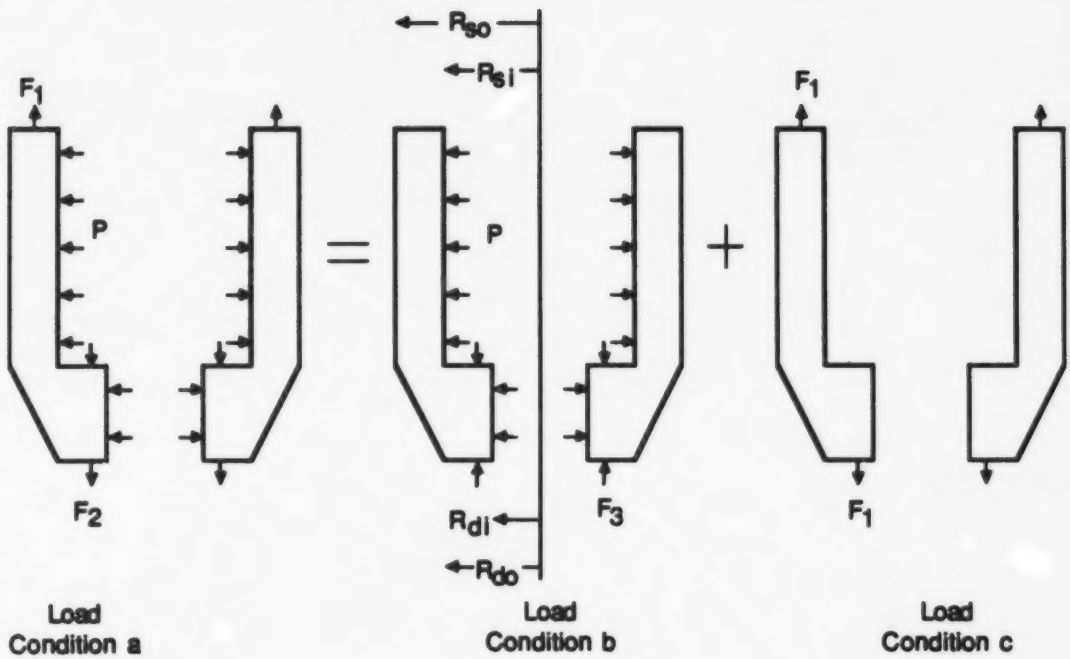

FIGURE A-1 Illustration of superposition of stresses.

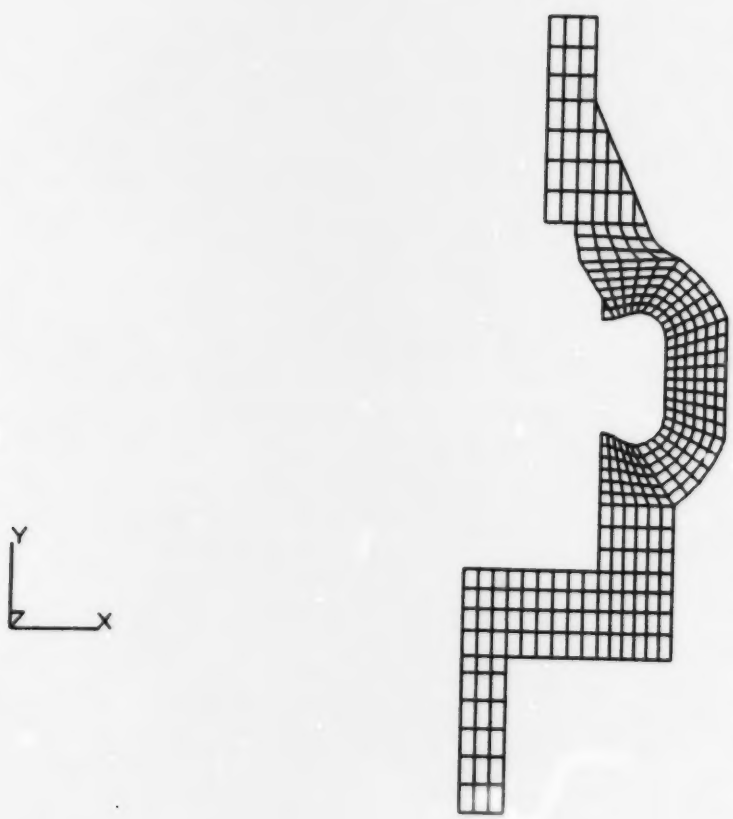

FIGURE A–2 Axisymmetric finite element model of Profile 1 of the pump casing.

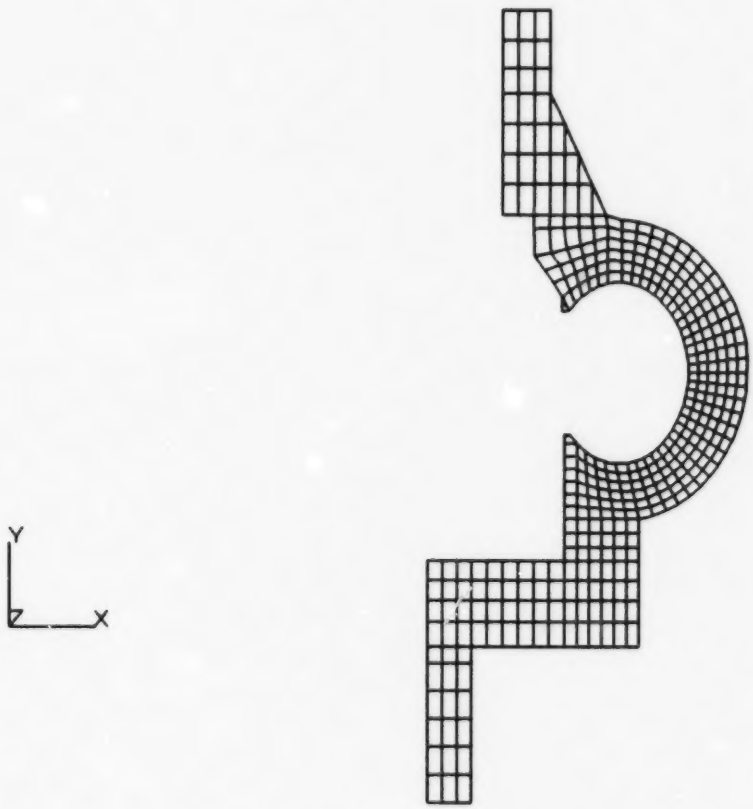

FIGURE A-3 Axisymmetric finite element model of Profile 2 of the pump casing.

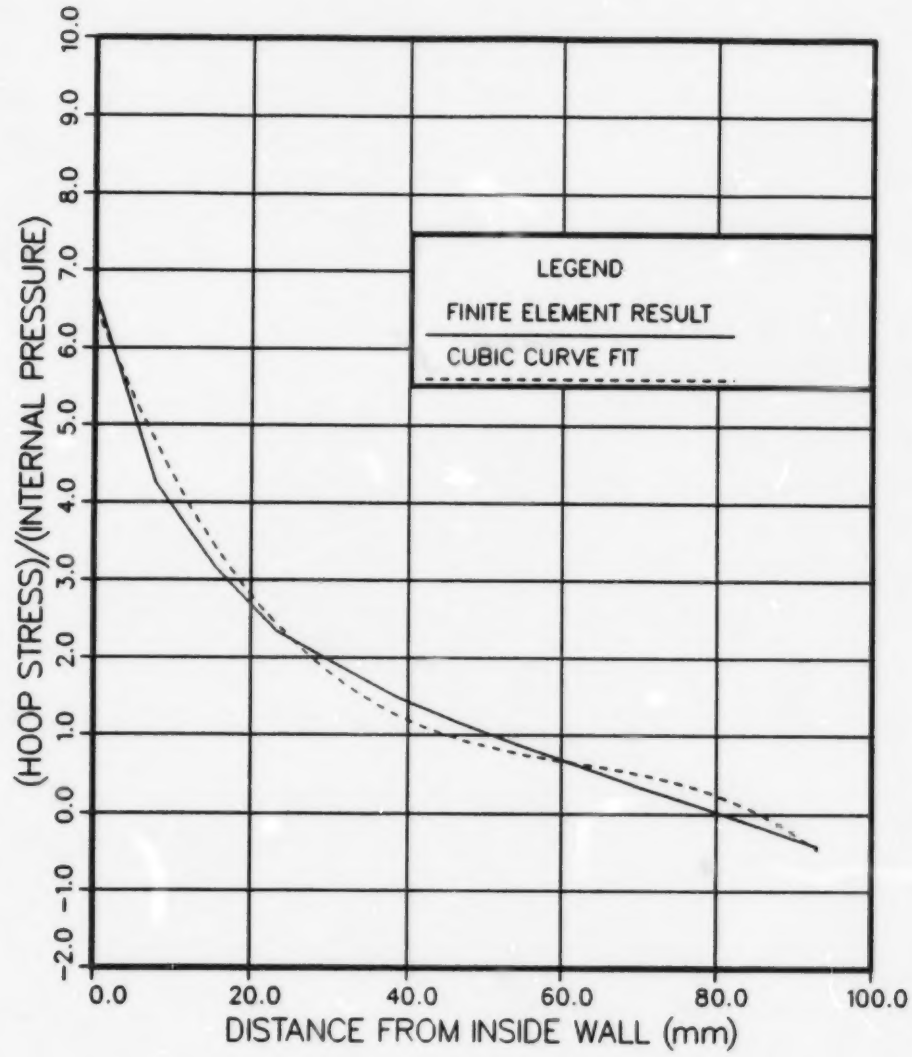

FIGURE A-4 Normalized normal stress distribution in the pump casing at Profile 1 - upper corner for internal pressure on the inside wall.

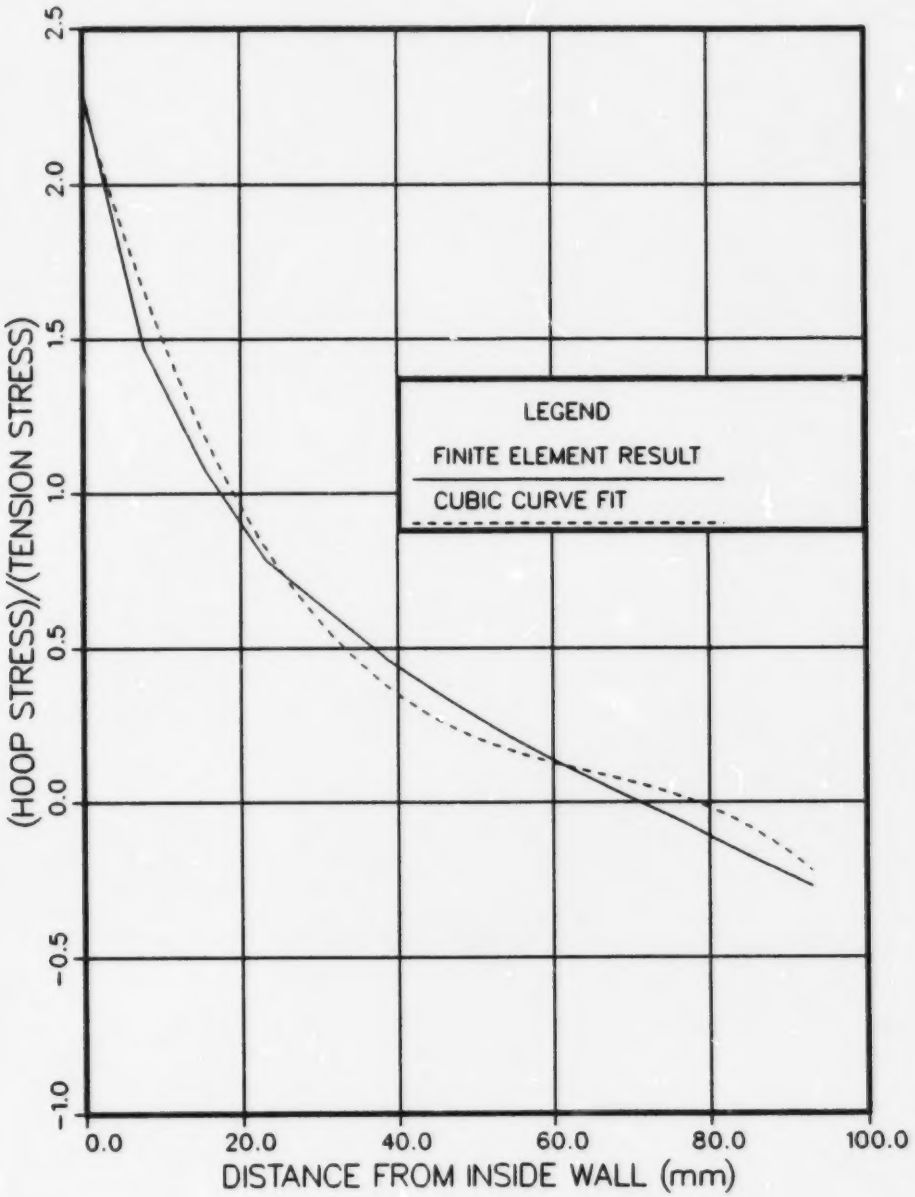

FIGURE A-5 Normalized normal stress distribution in the pump casing at Profile 1 - upper corner for tension on the suction end.

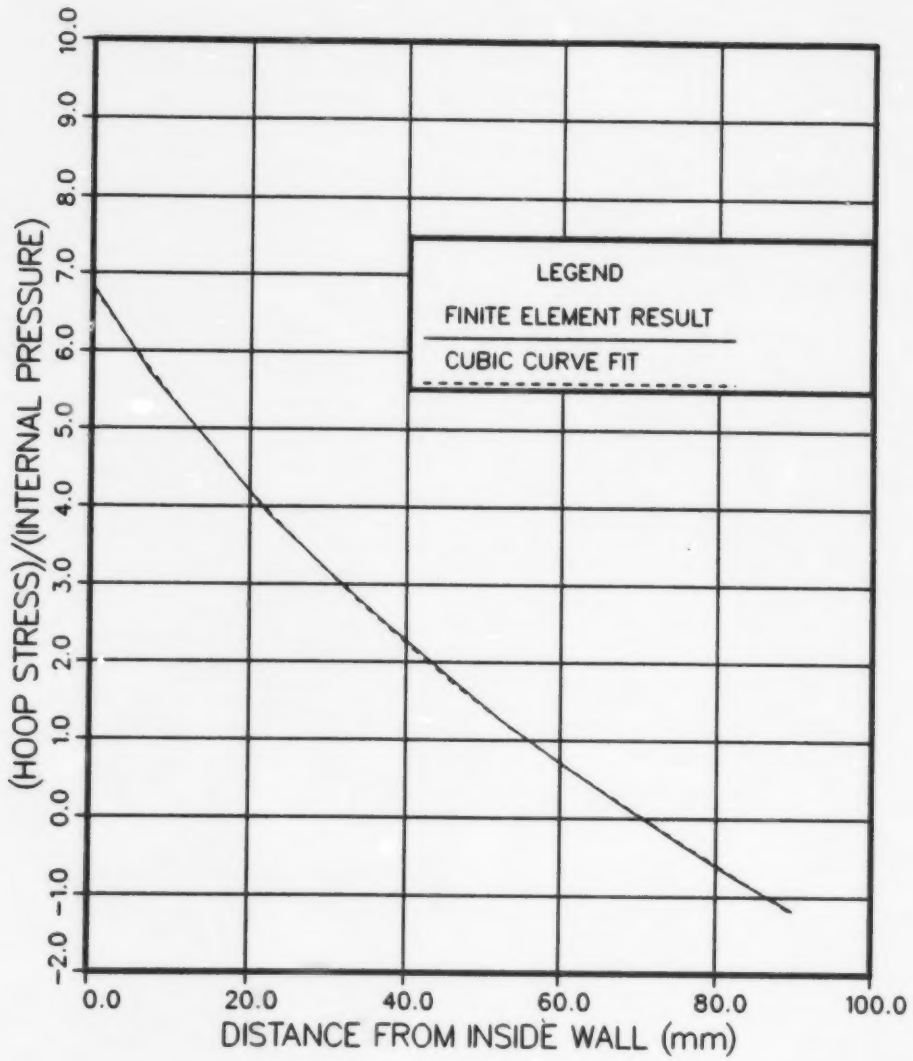

FIGURE A-6 Normalized normal stress distribution in the pump casing at Profile 2 - midsection for internal pressure on the inside wall.

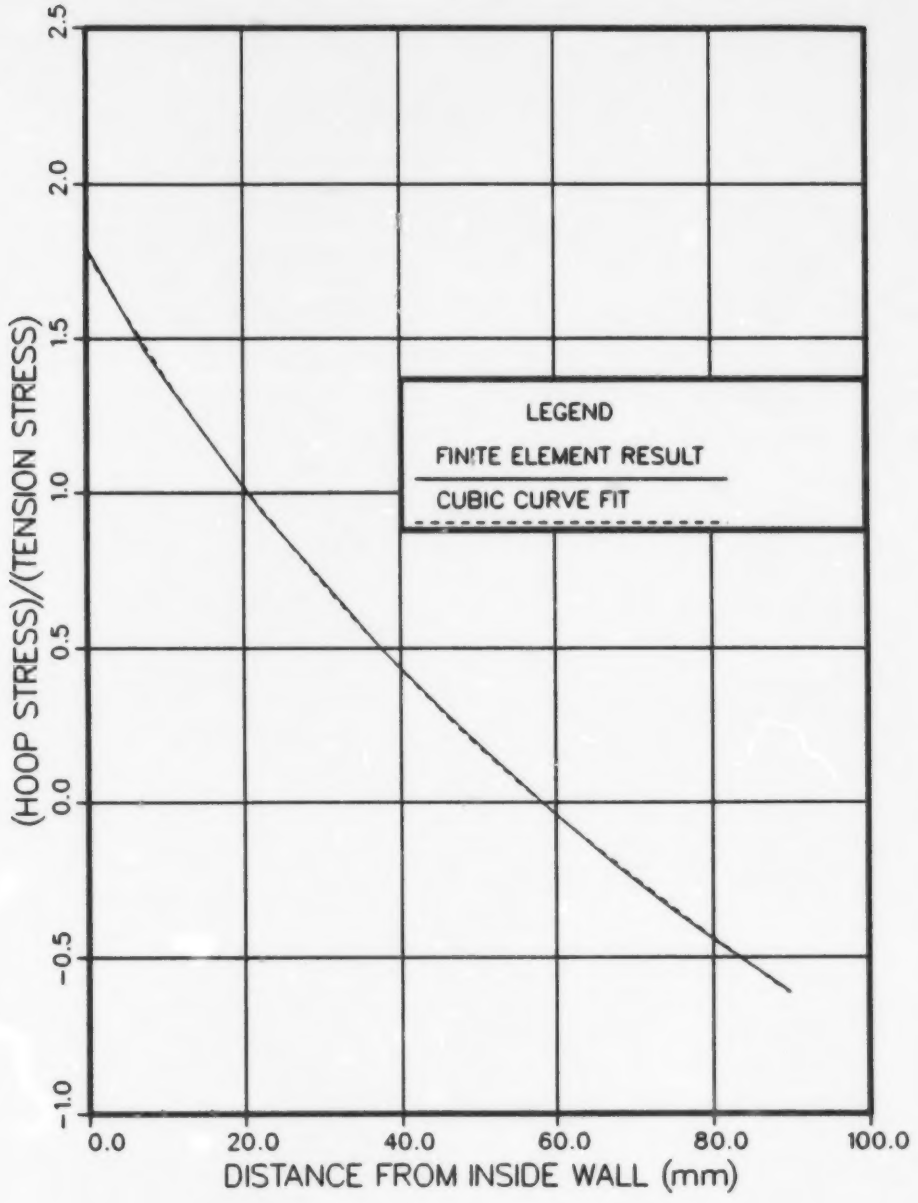

FIGURE A-7 Normalized normal stress distribution in the pump casing at Profile 2 - midsection for tension on the suction end.

APPENDIX B

Formulae for the Crack-Tip Stress Intensity Factor

The formulae are all based on an axial crack in a circular cylinder. See Figure 6–1.

B.1 Pump Casing

Infinite Aspect Ratio (a/c = 0.0)

The expression is taken from Buchalet and Bamford/12/.

$$K_I = (\pi a)^{0.5} [(A_0 + p)F_1 + (2a/\pi)A_1F_2 + (a^2/2)\ A_2F_3 + (4a^3/3\pi)A_3F_4] \quad \text{(B–1)}$$

where a = the crack depth,

p = internal pressure,

A_i = the cubic stress distribution coefficients given by equation (5–1),

F_i = the geometry influence coefficients, given in Table B–1.

The values of F_i were calculated in /12/ for an inner radius to wall thickness ratio, R_i/t, of 10 to 1. The application of these values of F_i to the pump casing, where R_i/t varies between 1 and 10, is considered to be slightly conservative. The internal pressure has been added to A_0 to account for pressure acting on the crack faces.

Aspect Ratio = 10 (a/c = 0.2)

The expression is taken from Raju and Newman/13/

$$K_I = (\pi a/Q)^{0.5} [(A_0 + p)G_0 + aA_1G_1 + a^2\ A_2G_2 + a^3\ A_3G_3] \quad \text{(B–2)}$$

where Q = the flaw shape parameter,

$$Q = 1 + 1.464\ (a/c)^{1.65}, \quad \text{(B–3)}$$

c = one–half the crack length,

p = internal pressure,

A_i = the cubic stress distribution coefficients given by equation (5–1),

G_i = the geometry influence coefficients taken from /13/ and given in Table B–2 for $R_i/t = 4$ and $a/c = 0.2$.

The internal pressure has been added to A_0 to account for pressure acting on the crack faces.

B.2 Discharge Valve Body

Infinite Aspect Ratio (a/c = 0.0)

The crack-tip stress intensity factor due to internal pressure is taken from Rooke and Cartwright/14/

$$K_I = (2pR_o^2/(R_o^2 - R_i^2))(\pi a)^{0.5} F_p \qquad (B-4)$$

where p = internal pressure,

R_i = the inner wall radius,

R_o = the outer wall radius,

F_p = the geometry influence coefficient taken from /14/ and given in Table B-3.

The crack-tip stress intensity factor for the thermal stress distribution is given by a reduced form of equation (B-1).

$$K_I = (\pi a)^{0.5} [A_{th0} F_1 + (2a/\pi)A_{th1}F_2] \qquad (B-5)$$

where A_{thi} = the linear thermal stress distribution coefficients given by equations (5-5) to (5-7),

F_i = the geometry influence coefficients given in Table B-1.

Aspect Ratio = 10 (a/c = 0.2)

The crack-tip stress intensity factor due to internal pressure is taken from Raju and Newman/13/.

$$K_I = p(R_o^2/(R_o^2 - R_i^2))(\pi a/Q)^{0.5} [2G_0 - 2(a/R_i) G_1 + 3(a/R_i)^2 G_2 - 4(a/R_i)^3 G_3] \qquad (B-6)$$

where p = internal pressure,

R_i = the inner wall radius,

R_o = the outer wall radius,

Q = the flaw shape parameter given by equation (B-3),

G_i = the geometry influence coefficients taken from /13/ and given in Table B-2 for $R_i/t = 4$ and $a/c = 0.2$.

The crack-tip stress intensity factor for the thermal stress distribution is given by a reduced form of equation (B-2).

$$K_I = (\pi a/Q)^{0.5} [A_{th0} G_0 + aA_{th1} G_1] \qquad (B-7)$$

where Q is defined above,

A_{thi} = the linear thermal stress distribution coefficients given by equations (5-5) to (5-7),

G_i = the geometry influence coefficients taken from reference /13/ and given in Table B-2.

TABLE B-1

Geometry Influence Coefficients for an Axial Crack With an Infinite Aspect Ratio Subject to a Cubic Hoop Stress Distribution (From Reference /12/)

Crack Depth/Wall Thickness	F_1	F_2	F_3	F_4
0.00	1.12	1.00	1.00	1.00
0.10	1.22	1.05	1.03	1.01
0.22	1.43	1.23	1.15	1.07
0.30	1.61	1.35	1.27	1.15
0.45	2.20	1.73	1.54	1.35
0.50	2.44	1.86	1.65	1.43
0.70	3.87	2.68	2.20	1.88
0.80	5.01	3.27	2.59	2.18

TABLE B-2

Geometry Influence Coefficients for an Axial Crack With an Aspect Ratio of 10 Subject to a Cubic Hoop Stress Distribution (From Reference /13/)

Coefficient	Deepest Point of Crack Penetration			Intersection of Crack with Free Surface		
	Crack Depth/Wall Thickness			Crack Depth/Wall Thickness		
	0.2	0.5	0.8	0.2	0.5	0.8
G_0	1.097	1.405	1.959	0.606	0.797	1.201
G_1	0.666	0.776	0.996	0.079	0.141	0.262
G_2	0.511	0.567	0.692	0.023	0.054	0.108
G_3	0.426	0.460	0.542	0.010	0.028	0.059

Based on $R_i/t = 4.0$, $a/c = 0.2$.

TABLE B-3

Geometry Influence Coefficients for an Axial Crack With an Infinite Aspect Ratio Under Internal Pressure (From Reference /14/)

Crack Depth/Wall Thickness	Inner Radius/Outer Radius	
	0.667	0.800
0.00	1.12	1.12
0.05	1.11	1.12
0.10	1.11	1.13
0.15	1.12	1.15
0.20	1.15	1.18
0.25	1.21	1.22
0.30	1.27	1.30
0.35	1.33	1.42
0.40	1.40	1.56
0.45	1.47	1.70
0.50	1.54	1.85
0.55	1.62	1.99
0.60	1.71	2.13
0.65	1.79	2.29
0.70	1.88	2.47
0.75	1.98	2.73

APPENDIX C

Crack Growth
Due to Mechanical Fatigue

The predicted curves of crack depth versus number of startup/shutdown cycles for Profiles 1 and 2 in the pump casing are given in Figures C–1 and C–2, respectively. The predicted curves for the discharge valve body with a wall thickness of 47 mm and 64 mm are given in Figures C–3 and C–4, respectively. The integration of equation (8–1) for the discharge valve body was started at the crack depth at which the crack would grow 1 mm in 10,000 cycles or less. This allowed the infinite aspect ratio and semi–elliptical crack to be plotted on the same linear–linear scales. The starting depths of the less severe semi–elliptical cracks are therefore greater than the starting depths of the infinite aspect ratio cracks. The purpose of these curves is to estimate the crack growth increment for any postulated crack depth and given number of cycles, as described in the next paragraph. A plot of the curves for the two crack shapes on the same figure illustrates the higher crack growth rates for the infinite aspect ratio cracks.

The fatigue crack growth can be estimated from these curves for any initial crack depth by following the procedure illustrated in Figure C–5. From the initial crack depth a_1, the reference cycle number N_1 is found from the curve. The final cycle number N_2 is given by N_1 plus the estimated number of future cycles ΔN. From the curve, the estimated final crack depth is then determined. Due to the uncertainty of the application of the ASME Section XI water environment curve to the Lambton TGS environment, some factor of safety must be imposed on the fatigue crack growth.

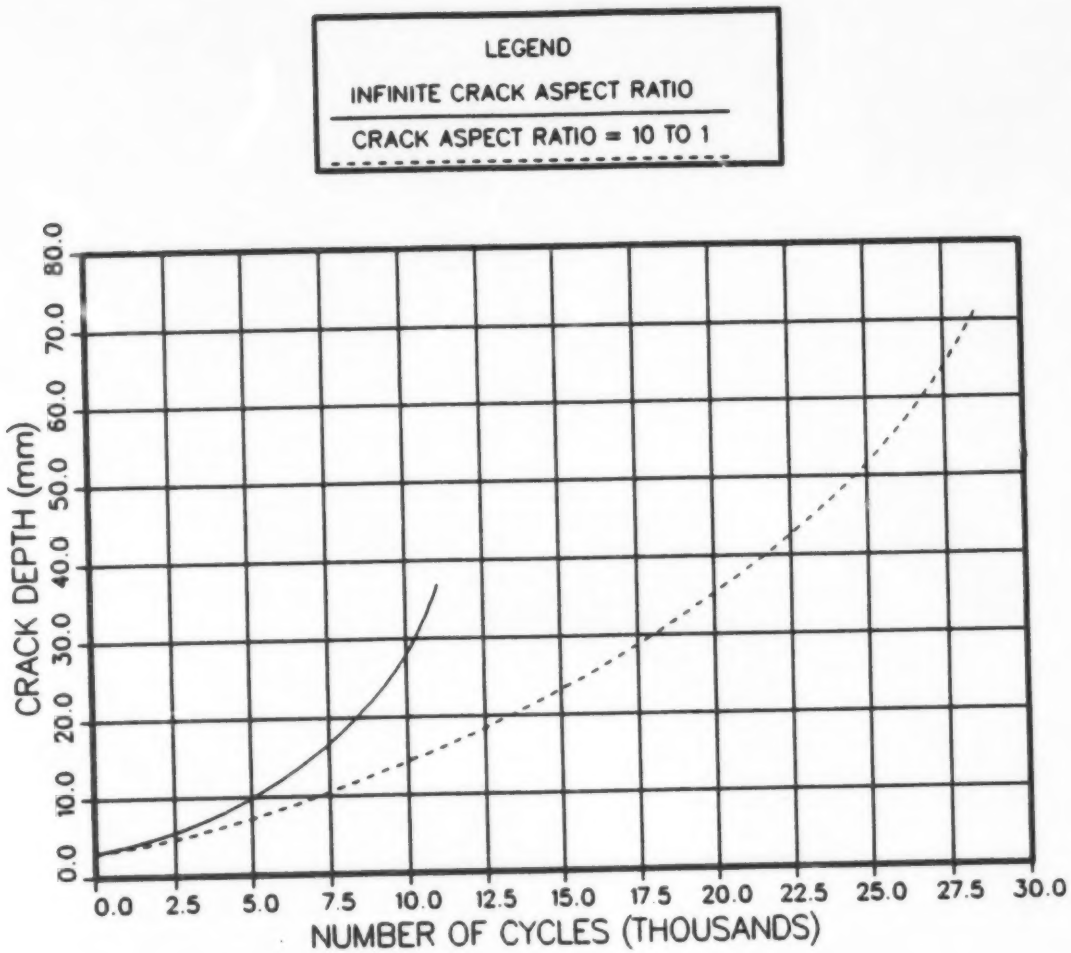

FIGURE C-1 **Integrated fatigue crack growth for Profile 1 in the pump casing.**

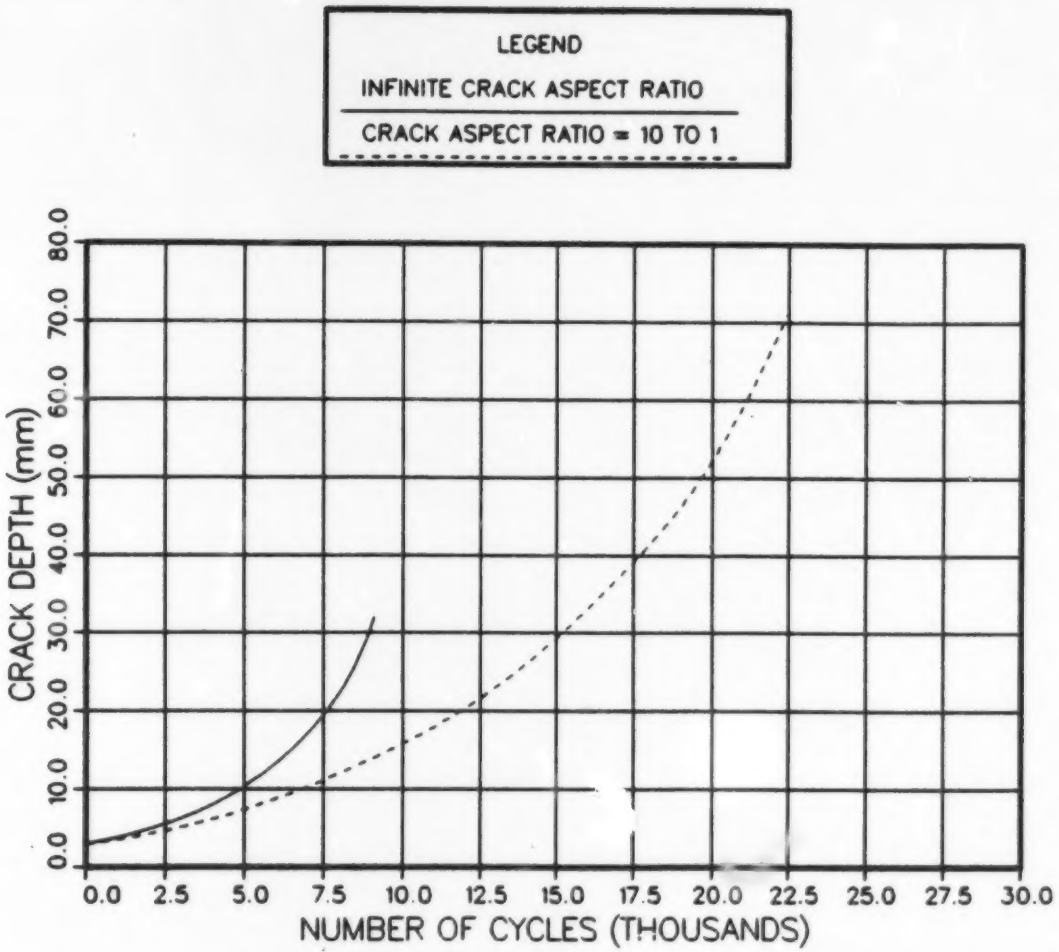

FIGURE C-2 **Integrated fatigue crack growth for Profile 2 in the pump casing.**

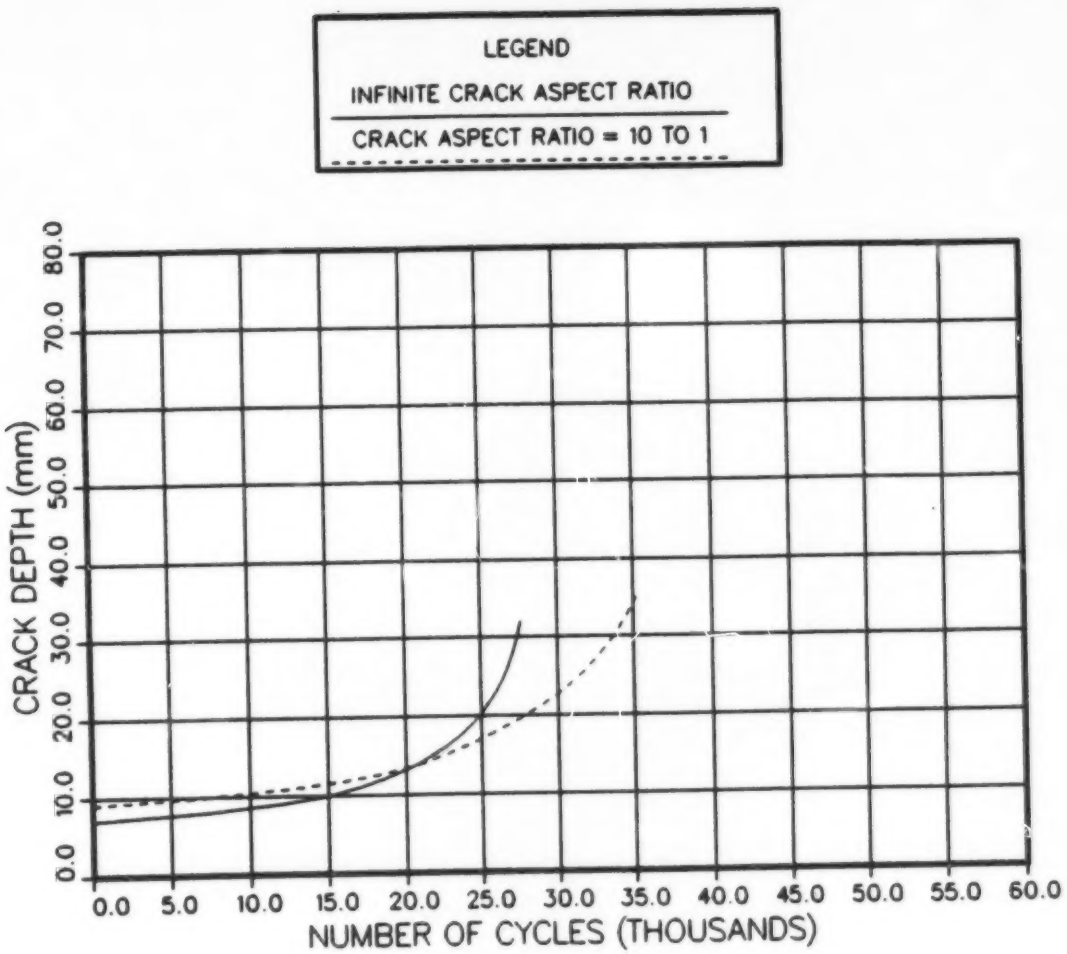

FIGURE C-3 **Integrated fatigue crack growth for a discharge valve body with a wall thickness of 47 mm.**

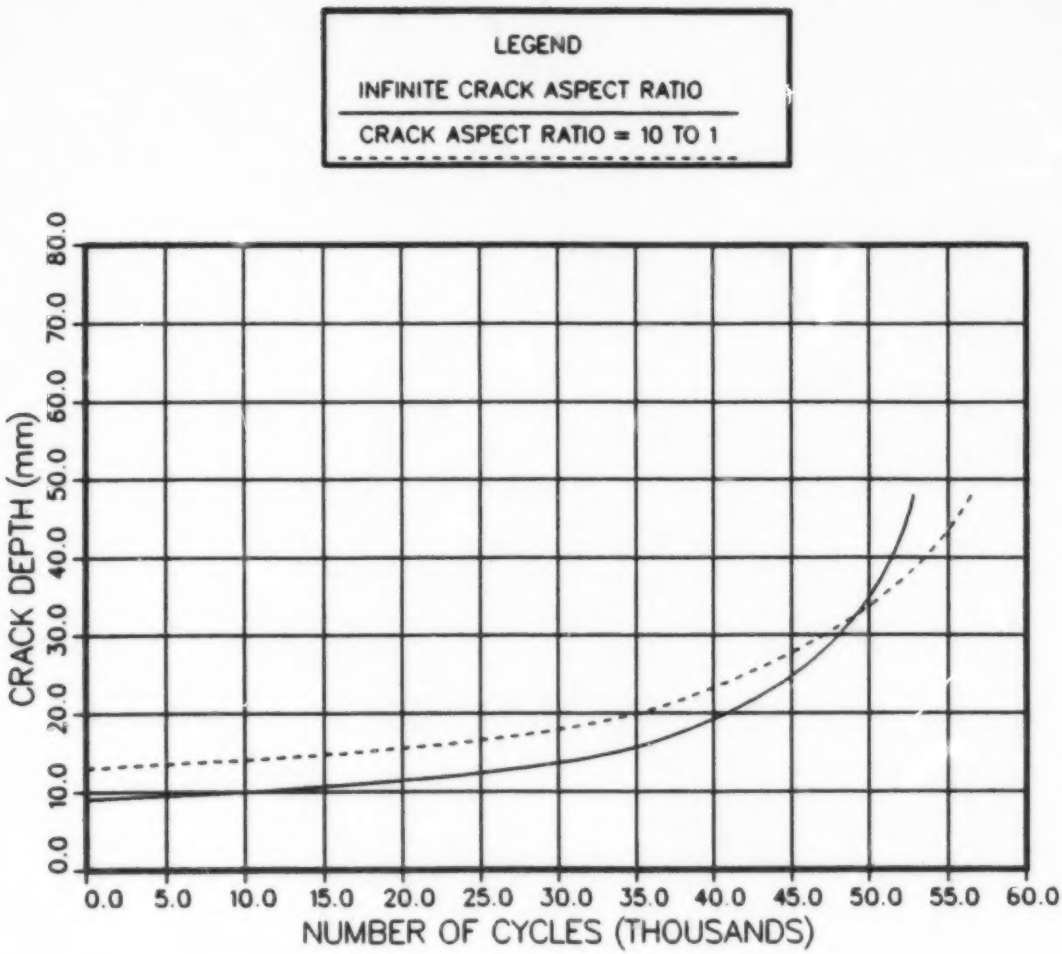

FIGURE C-4 **Integrated fatigue crack growth for a discharge valve body with a wall thickness of 64 mm.**

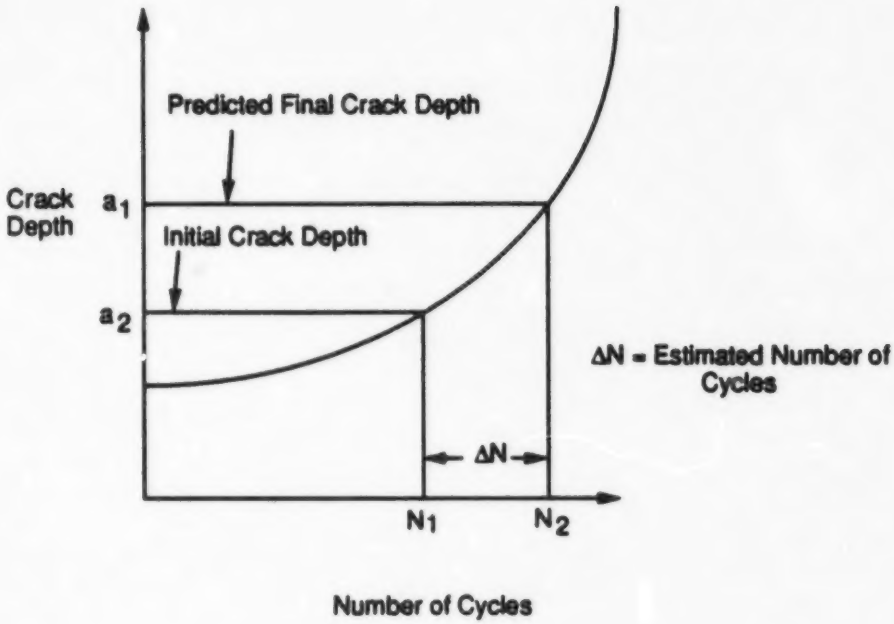

FIGURE C-5 Illustration of estimation of fatigue crack growth.